NMR-based isotopic and isotopomic analysis

Serge Akoka, Gérald S. Remaud

NMR-based isotopic and isotopomic analysis

Serge Akoka*, Gérald S. Remaud

Université de Nantes, CNRS, CEISAM UMR 6230, F-44000 Nantes, France

***Corresponding author**: Serge AKOKA

Chimie et Interdisciplinarité: Synthèse, Analyse, Modélisation (CEISAM), UMR 6230, Faculté des Sciences, BP 92208, 2 rue de la Houssinière, F-44322 Nantes Cedex 03, France.

Tel. +33(0)2 51 12 57 07 ; E-mail: serge.akoka@univ-nantes.fr

Gerald Remaud, Chimie et Interdisciplinarité: Synthèse, Analyse, Modélisation (CEISAM), UMR 6230, Faculté des Sciences, BP 92208, 2 rue de la Houssinière, F-44322 Nantes Cedex 03, France.

Tel. +33(0)2 51 12 57 19 ; E-mail: gerald.remaud@univ-nantes.fr

72 Pages 25 figures 3 tables

Key words: Isotopic analysis, irm-NMR, Quantitative NMR, High accuracy, PSIA

Abstract

Molecules exist in different isotopic compositions and most of the processes, physical or chemical, in living systems cause selection between heavy and light isotopes. Thus, knowing the isotopic fractionation of the common atoms, such as H, C, N, O or S, at each step during a metabolic pathway allows the construction of a unique isotope profile that reflects its past history. Having access to the isotope abundance gives valuable clues about the (bio)chemical origin of biological or synthetic molecules. Whereas the isotope ratio measured by mass spectrometry provides a global isotope composition, quantitative NMR measures isotope ratios at individual positions within a molecule. We present here the requirements and the corresponding experimental strategies to use quantitative NMR for measuring intramolecular isotope profiles. After an introduction showing the historical evolution of NMR for measuring isotope ratios, the vocabulary and symbols - for describing the isotope content and quantifying its change - are defined. Then, the theoretical framework of very accurate quantitative NMR is presented as the principle of Isotope Ratio Measurement by NMR spectroscopy, including the practical aspects with nuclei other than ^{2}H, that have been developed and employed to date. Lastly, the most relevant applications covering three issues, tackling counterfeiting, authentication, and forensic investigation, are presented, before giving some perspectives combining technical improvements and methodological approaches.

Table of contents

1. Introduction 5

2. Isotopic analysis 10

2.1. Isotopologues, isotopomers and isotopic quantities 10

2.2. Isotope fractionation 11

2.3. Interest of NMR for isotope analysis 13

3. High accuracy quantitative NMR 17

3.1. Trueness, precision and accuracy 17

3.2. Is NMR always quantitative? 17

3.3. Parameters influencing trueness 18

3.4. Parameters influencing precision 23

3.5. Experimental conditions for high accuracy quantitative NMR 27

4. Isotope ratio measurement by NMR 30

4.1. Isotopic fingerprinting 30

4.2. Position-specific isotope abundance measurement 30

4.3. Practical aspects 35

5. Applications 38

5.1. Sample preparation 38

5.2. Counterfeiting 40

5.3. Forensic investigations 44

5.4. Authentication 50

5.5. Multi-omics approach 56

6. Concluding remarks and perspectives 59

Acknowledgements 61

References 62

Glossary of abbreviations 69

Acronyms and notations for NMR 69
Isotope terms 70
Other notations 71

1. Introduction

Molecules exist in different isotopic compositions in which the heavy element distributions depend on the processes and raw materials used for making the component. Most of the processes, physical or chemical, in living systems cause selection between heavy and light isotopes. Thus, knowing the isotopic fractionation of the common atoms, such as H, C, N, O or S, at each step during a synthetic or metabolic process leads to the construction of a unique isotope profile that reflects the past history of the molecule. Having access to the isotopic abundances gives valuable clues about the (bio)chemical origins of molecules [1].

There are several techniques for determining isotope ratios [2 and refs. within]. Mass spectrometry (irm-MS: isotope ratio measurement by Mass Spectrometry, also known as IRMS: Isotope Ratio by Mass Spectrometry) was used first. Irm-MS is designed to measure the isotope abundance in targeted gases introduced into the source of the spectrometer. For example, CO_2 and N_2 are the gases used to determine $^{13}C/^{12}C$ and $^{15}N/^{14}N$ ratios. Organic matter is converted into these gases via the successive oxidation and reduction furnaces of an elemental analyzer. Then, the ratios $^{13}CO_2/^{12}CO_2$ or $^{15}N_2/^{14}N_2$ are measured after appropriate calibrations, and the result is expressed as the global (or bulk) isotopic composition: $\delta^{13}C_g$ and $\delta^{15}N_g$ (see Section 2 for definitions of symbols). Irm-MS has two main advantages: instrumental automation, and the requirement for only a small amount of material (routinely a few mg) [3]. Later, hyphenated methodologies were developed, such as chromatographic coupling: liquid chromatography (LC-irm-MS) and, mainly, gas chromatography (GC-irm-MS), leading to so-called CSIA (Compound Specific Isotope Analysis) [4].

However, only the average contribution of all the ^{13}C or ^{15}N isotopomers and isotopologues (these and other relevant terms are explained in section 2) present in the compound is determined leading to one overall parameter, $\delta^{13}C_g$ or $\delta^{15}N_g$. The intramolecular isotope distribution is thus not accessible, unless indirect measurements are made on fragments. The oldest approach to position-specific isotope analysis (PSIA) is the chemical and/or enzymatic degradation of the molecule, with

subsequent analysis of the resulting fragments by irm-MS. A less tedious methodology was developed through on-line pyrolysis and GC separation of fragments coupled with mass spectrometry [5]. However, this is currently restricted to small molecules such as acetic acid, lactic acid or ethanol [6].

Whereas the isotope ratio measured by Mass Spectrometry (irm-MS) provides a global isotope composition, *e.g.* $\delta^{13}C_g$, quantitative NMR measures isotope ratios at individual positions (sites) of a molecule (irm-NMR: isotope ratio measured by NMR, also known as SNIF-NMR^{TM}: Site-Specific Natural Isotope Fractionation determined by NMR). By separating and quantitating each isotopomer, irm-NMR resolves isotope fractionation at natural abundance for every position in target molecules. Historically, the use of NMR spectroscopy for isotope ratio measurement was pioneered by Martin and Martin in the early 1980s, applying quantitative ^{2}H NMR to ethanol for the detection of over-chaptalized wines [7]. Despite its very low sensitivity, deuterium has some favorable characteristics for quantitative NMR: (i) the predominance of quadrupolar relaxation avoids perturbations in signal intensities due to the nOe (nuclear Overhauser effect), (ii) longitudinal relaxation times (T_1) are not too long and (iii) the large array of isotope effects (isotopic composition range around 500‰) means that the precision needed for irm-^{2}H NMR is only of the order of a few percent. As a result, various applications have been published over the last 30 years in areas covering the authenticity of flavors and food, counterfeiting of medicines, and forensic investigations [8]. In 1988, irm-^{2}H NMR was adopted by the International Office of Vines and Wine (OIV) and by the EEC and became the official method to detect sugar addition in wine, and to determine the origins of vanillin and acetic acid [8]. A remarkable development of irm-^{2}H NMR was achieved in chirally oriented media, which makes accessible residual anisotropic intramolecular NMR interactions while preserving high spectral resolution. In such an environment, enantiomers of chiral molecules or enantiopic elements of prochiral produce distinct NMR signals, giving access to unique information. That led to a fundamental understanding of the enzymatic processes (stereoselectivity) of natural ^{2}H distribution in prochiral molecules [9].

Nevertheless, there are some limitations of irm-^{2}H NMR that are not (or are only partly) compensated by using a very high magnetic field and cryoprobe. The amount of material needed for analysis is relatively high, *e.g.* 1 g for irm-^{2}H NMR on vanillin in routine analysis on a 400/500 MHz spectrometer, prohibiting the study of minute amounts of compound. Furthermore, the hydrogen atom (and therefore ^{2}H) is often easily exchangeable. These and other problems of irm-^{2}H NMR have been circumvented by studying nuclei such as ^{13}C or ^{15}N. However, the performance that must be reached to determine isotope ratios is 10 times higher for ^{13}C (or for ^{15}N) than for ^{2}H, since the range of variability of ^{13}C isotopic compositions is restricted to 50‰ in natural products, leading to a required precision better than 1‰ (or 0.1%) [10]. For comparison, the precision of irm-MS is 0.3‰ in routine analysis for the determination of $\delta^{13}C_g$ on organic matter. During the same period as ^{2}H NMR was being developed, several attempts were made to establish a methodology for irm-^{13}C NMR with reproducible data, but these achieved only moderate results [11, 12]. However, 15 years ago the major source of irreproducibility was identified as the efficiency of the ^{1}H decoupling, because of its variation over the range of proton frequencies. Once this obstacle had been overcome, reproducible results were obtained [13, 14] on reduced amounts of sample, providing valuable further information compared to ^{2}H NMR. The method was named irm-^{13}C NMR 'single-pulse' (^{13}C excitation followed by inverse gated decoupling, as opposed to the multi-pulse methodology). For example, the analysis of vanillin can be performed on 250 mg, instead of 1 g for irm-^{2}H NMR, with even more discriminating parameters [15]. The application of this single-pulse approach provided a range of results not previously accessible, including the counterfeiting of active pharmaceutical ingredients (APIs), the metabolism of photosynthesis and post-photosynthesis, the authenticity of natural products, and sorption and evaporation phenomena.

The most outstanding finding from these data was the occurrence of normal (^{12}C is favored) and inverse (^{13}C is favored) isotope effects during the same process. In addition, long-range isotope effects were also observed. Advanced modeling of isotope fractionation and mechanisms of transformation confirmed that the intramolecular isotope distribution provides many more details,

which could be missed when using the global value from irm-MS. A strong argument can then be put forward to answer the question: if there is no change in $\delta^{13}C_g$ during a transformation (between substrate and product), does this mean that there is no fractionation within the molecule? The answer given by PSIA is usually no, because there is a counteractive contribution of normal and inverse intramolecular isotope effects at different positions, generating an average close to zero.

Despite these important contributions, the single-pulse method has some limitations, because the amount of pure molecule required remains too high and the analysis duration too long for many applications. Clearly, an increase in molecular weight will make irm-^{13}C NMR 'single-pulse' difficult. In contrast to ^{2}H, because ^{13}C has a spin of ½, it is easy to use multi-pulse sequences for sensitivity and/or resolution improvement. The challenge inherent in achieving the high precision (about 1‰) required for isotopic measurement is: what are the modifications that should be made to a pulse sequence to achieve exact and robust data? This is particularly important for refocusing and inversion with π pulses. A thorough investigation of the polarization transfer sequences, namely DEPT and INEPT, showed that adiabatic pulses provide robust and very reproducible ^{13}C profiles in a short time or with less product. With shorter repetition time (TR) and polarization transfer, a gain in sensitivity of six- to ten-fold can be obtained depending on the studied molecule [16].

However, with such sequences, quaternary carbons are not observed, and the intensity of a signal depends on the values of the delays used in the polarization transfer. This is to say that the area of the signal is not solely proportional to the number of nuclei giving this signal, but also depends on pulse sequence parameters. Nevertheless, this apparent isotope composition (see Section 4.2 for further details) will change from one sample to another due to the change in the ^{13}C amount. The resulting profiles can be used as input data for omics interpretation: the concept of isotopomics at natural abundance was then introduced (this term was first used for mapping the isotopic distribution over metabolites upon ^{13}C labeling [17]). In some cases, the number of quaternary carbons is not negligible and information is undoubtedly lost. The delay for the transfer of polarization in INEPT can be adjusted to long-range ^{1}H-^{13}C couplings ($^{n}J_{13C\text{-}1H}$). The resulting

153 methodology was named Full-Spectrum INEPT (FS-INEPT) [18]. It was tested for ^{13}C profiling (showing
154 that full ^{13}C profiles could be obtained for 40 mg of caffeine or acetaminophen in a short time) as
155 well as for ^{15}N [19] for which it is the only way to observe isotope effects.

156 The present article aims to present the requirements and the corresponding experimental strategies
157 for using quantitative NMR to measure intramolecular isotope profiles. Several questions are
158 addressed in order to help the reader identify both the potential and the constraints of isotope ratio
159 measurement by NMR spectroscopy (irm-NMR). (i) What are the areas of interest for isotope
160 composition? (ii) How is the isotope content expressed? (iii) What is measured according to the
161 technique used? (iv) What are the conditions for quantitative NMR to reach appropriate accuracy?
162 (v) Are there typical examples of applications of irm-NMR?

163 In this review, the answers to these questions are organized as follows: after this Introduction
164 describing the historical evolution of NMR for measuring isotope ratios, we define in Section 2 the
165 vocabulary and symbols used for describing the isotope content and for quantifying its change.
166 Section 3 covers the theoretical framework of quantitative NMR within the constraint of a very high
167 accuracy level, defined as trueness and precision. In Section 4, we detail the principle of isotope ratio
168 measured by NMR spectroscopy (irm-NMR), including practical aspects with nuclei other than ^{2}H,
169 that have been developed and employed to date. In Section 5, we present and discuss the most
170 relevant applications covering three issues: tackling counterfeiting, authentication and forensic
171 investigation. In that Section, we also stress the rules for preparing samples without isotope
172 fractionation. Finally, we conclude with some perspectives combining technical improvements and
173 methodological approaches.

174

2. Isotopic analysis

2.1. Isotopologues, isotopomers and isotopic quantities

As mentioned in the Introduction, heavy isotopes, such as ^{2}H or ^{13}C, are not uniformly distributed in a molecule; this leads to different isomers which are called isotopologues. When two isotopologues have the same number of positions occupied by a given isotope, they are called isotopomers (**Fig. 1**).

In the case of light elements (H, C, N, O), the average abundances of heavy isotopes are small and so the probability of finding two heavy isotopes in the same isotopologue is very low. Consequently, most isotopologues detected by NMR at natural abundance are mono-labeled isotopomers.

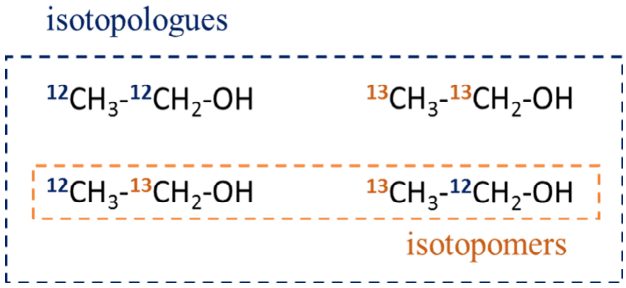

Fig. 1: Difference between isotopologues and isotopomers, illustrated for carbon atoms in ethanol. Isotopologues differ only in their isotope compositions, whereas isotopomers have the same numbers of isotopes but in different positions. Reprinted with permission from Ref. [21]. Copyright 2017 Magnetic Resonance in Chemistry.

In order to quantify the isotope distribution between different molecules or within a given molecule, different expressions are routinely used (**Table 1**). For the element *E*, the isotope ratio (R) measures the relative amount of the heavier isotope (^{h}E) compared to the lighter one (^{l}E), while the isotope abundance (x) measures the relative amount of the heavier isotope (^{h}E) compared to the total amount of element *E* [20]. It should be noted that for hydrogen and oxygen, the isotope ratio and

isotope abundance have almost the same value because of the very small amount of heavy isotopes, but this is not the case for all elements, notably carbon.

For carbon and nitrogen, the range and variation of values observed are very small (a few percent), therefore it is preferable to use isotope composition (δ). This expresses the relative value (in permil, ‰) of the isotope ratio against an international standard (**Table 1**) [21].

Table 1: Relations defining the main expressions used in isotope analysis for an element *E* with two isotopes. The heavier and lighter isotopes are noted ${}^{h}E$ and ${}^{l}E$, respectively. *Std* indicates the international standard used to express the δ value.

Isotope ratio (R)	Isotope abundance (x)	Isotope composition (δ)
$R\left({}^{h}E/{}^{l}E\right) = \frac{N\left({}^{h}E\right)}{N\left({}^{l}E\right)}$	$x\left({}^{h}E/{}^{l}E\right) = \frac{N\left({}^{h}E\right)}{N\left({}^{h}E\right) + N\left({}^{l}E\right)}$	$\delta^{h}E_{std} = \left(\frac{R\left({}^{h}E/{}^{l}E\right)}{R\left({}^{h}E/{}^{l}E\right)_{std}} - 1\right).1000$

For the NMR community, this δ should not be confused with the use of δ for chemical shifts. The standard compounds employed are Vienna Pee Dee Belemnite and atmospheric N_2 (standard calibrated by IAEA (Vienna)) for ^{13}C and ^{15}N, respectively, although these are now routinely used via a calibrated intermediate compound.

2.2. Isotope fractionation

The fractionation between heavy and light isotopes is the result of the kinetic and thermodynamic isotope effects that lead to the selection of one isotope in preference to the other. As described in Section 2.1, isotopologues can differ in: (i) the type of elements and the corresponding isotopes; and/or (ii) the isotope itself; and/or (iii) the number of atoms of isotope; and/or (iv) the isotope positions within the molecule. All these molecules can behave differently according to the process involved: different masses result in different bond frequencies that lead to different zero-point

energies and therefore to changes in rates and in equilibria. Without going deeply into the theoretical aspects, it will suffice here to describe the essentials needed to understand what is measured and for what purpose [23]. The vibrational zero-point energy is lower for a bond involving a heavier isotope of an element, *i.e.* such bonds will be stronger. The energy of the system is minimized when the heavy isotope is at the position with the strongest bond. This is what is observed at equilibrium. Thus, we can distinguish the kinetic isotope effect (KIE) from the equilibrium isotope effect (EIE). In general, there are other contributions to the kinetic effect during a chemical reaction (steric, vibrational modes) usually leading to the normal isotope effect, in which the light species is favored, or the inverse isotope effect, in which the heavy species is favored (in this case, there is probably a contribution from a process at equilibrium). Depending on the scientific field, the isotope fractionation is expressed in different ways. The isotope effect is named α. During a transformation between A and B, α is given by Eq. (1):

$$\alpha_{A-B} = \frac{R_A}{R_B} \quad (1)$$

For a kinetic isotope effect, R_A is the isotope ratio of the substrate A and R_B that of the product obtained during a first-order reaction from A. For a thermodynamic effect (equilibrium), A is in equilibrium with B and the isotope ratios R are those at equilibrium. In biology, the fractionation is expressed as $\Delta = \alpha - 1$, where $\alpha > 1$ corresponds to a normal effect ($\Delta > 0$) and $\alpha < 1$ to an inverse effect ($\Delta < 0$). In geoscience, the fractionation is related to the enrichment factor ε by Eq. (2):

$$\varepsilon = (\alpha - 1) \times 1000 \quad (2)$$

However, in this case, α is the reverse of the previous one used in biological studies, and ε should be considered as $\varepsilon = -\Delta$. This will also invert the definition of the sense of fractionation. Readers of the publications cited in this review should be aware of the particular convention used for the work being described, by checking what rules are used by the authors to define a 'normal' or an 'inverse' isotope effect.

We present herein only one type of fractionation, that is relevant for interpreting applications related to plant origins: the photosynthetic pathways, *i.e.* the change in $\delta^{13}C$ according to the mechanism involved during the assimilation of atmospheric CO_2 during photosynthesis [10]. There are three metabolic processes, known as C_3, C_4 and CAM. This notation is associated with the number of carbon atoms of the molecule first synthesized upon carboxylation: for C_3 it is 3-phosphoglycerate (direct Calvin cycle); for C_4 it is oxaloacetate (intermediate prior to the Calvin cycle). The third strategy, CAM (Crassulacean Acid Metabolism), is an adaptation of the plant to water stress and is similar to C_4 but with different activity during night and day, associated with stomatal conductance: a contribution to the direct Calvin cycle is then possible, but via the C_4 mechanism. A very characteristic ^{13}C fractionation relative to the $\delta^{13}C$ of atmospheric CO_2 is found [24] for each photosynthetic pathway, that is constant over the earth, *i.e.* ≈ -8‰. A global fractionation of the order of -20‰ and -4‰ is observed for C_3 and C_4 plants, respectively, *e.g.* $\delta^{13}C_g$ ≈ -26 to -29‰ and ≈ -10 to -12‰ for sucrose in beet (C_3) and in sugar cane (C_4), respectively. For CAM plants, the fractionation depends on the plant and may be around -20‰, as for vanilla ($\delta^{13}C_g$ of vanillin ex-bean = -20‰), or close to the C_4 plant value, as for pineapple ($\delta^{13}C_g$ ≈ -12‰ of sugars in pineapple juice).

2.3. Interest of NMR for isotope analysis

In routine isotope analysis, global isotope abundance (x_g) is determined, most often using irm-MS [25, 26]. The main problem here is that isotope fractionation induces an intramolecular difference in the isotope amount, which can only be observed if the contribution at each position can be distinguished. In fact, the effect on the isotope ratio from a given position is diluted by the isotope ratios at all the other positions of the compound. It can thus fall below the detection threshold as soon as the molecule contains more than five or six carbons [27].

Several methods have been proposed to measure position-specific isotope compositions. The earliest involved chemically cleaving the analyte then analyzing the fragments separately by irm-MS [28]. More recently, GC-irm-MS was modified to perform position-specific isotope analysis (PSIA) [29] but

to date this technique is limited to molecules with a small number of carbons. High resolution mass spectrometry has also been adapted to measure clumped and position-specific isotope compositions [30]. It works on a very small sample but, like the previous method, MS-based isotope analysis is limited to small organic molecules. Furthermore, isotope fractionations that occur during analysis have not been successfully addressed. Therefore, the accuracy of this method has not yet been assessed by other proven methods.

On the other hand, NMR is an excellent method to perform PSIA since each isotope can be measured separately using its own resonance frequency, and each molecular position can be distinguished by its chemical shift (**Fig. 2**). Moreover, peak areas are directly proportional to the number of detected nuclei, and therefore to the isotope abundance (x_i) of the considered position i. The signal detected for position i is given by Eq. (3):

$$S_i = k.n_i.c.x_i \quad (3)$$

where n_i is the number of equivalent nuclei at position i and c the concentration of the measured compound.

The molar fraction of each isotopomer can then be calculated using Eq. (4) [31]:

$$f_i = \frac{S_i}{\sum S_i} \quad (4)$$

The set of f_i provides an isotopic profile directly, which can be used to trace or authenticate a compound [21, 22, 31]. It can also be used to obtain the specific abundances using two methods [31]. Either a reference compound of known isotope abundance is added to the sample, or the global isotope abundance x_g is obtained by a method other than NMR. These two approaches are developed in Section 4.

However, this is only possible if the measurement accuracy is better than the variations observed in isotope abundance at natural abundances. The performance to be reached for the determination of isotope ratios is 10 times higher for ^{13}C (or for ^{15}N) than for ^{2}H, since the range of variability of the

isotopic ^{13}C compositions is restricted to 50‰ in natural products, leading to a required precision better than 1‰ (or 0.1%). For comparison, the precision of irm-MS is 0.3‰ in routine analysis for the determination of $\delta^{13}C_g$ [21, 22, 31].

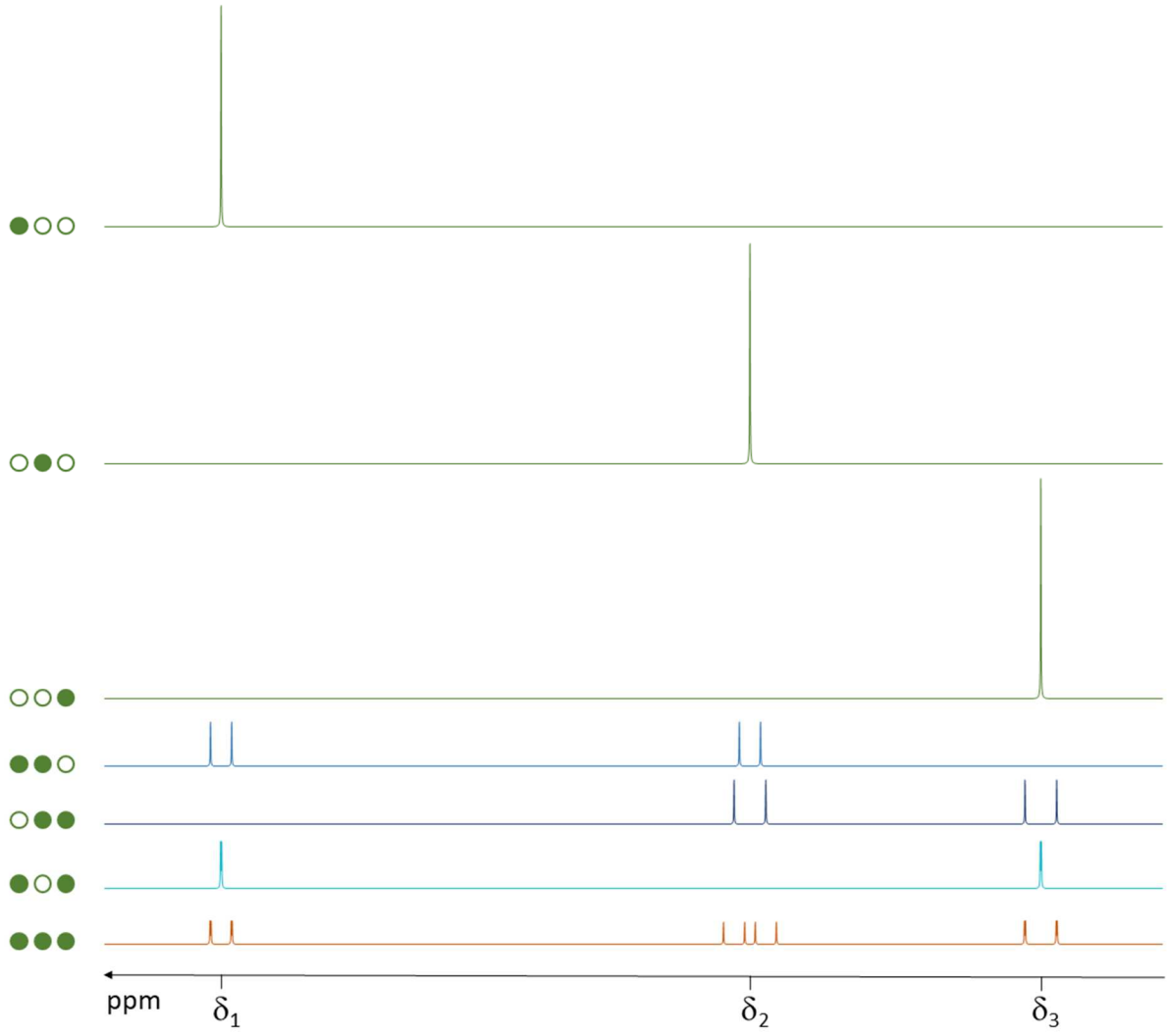

Fig. 2: ^{13}C-NMR signals from a three-carbon molecule. Filled circles indicate positions occupied by a ^{13}C and open circles indicate positions occupied by a ^{12}C. The contributions of bi-labelled isotopologues are equivalent and are assumed to be close to the average abundance 1.1% each, since NMR will not be able to distinguish small variations around this average value. Signal from the tri-labelled isotopologue theoretically contributes but its abundance is too low to be detected by NMR with current techniques. The observed spectrum consists in the addition of all these contributions.

This explains why ^{2}H was the first nucleus used for irm-NMR. However, as previously mentioned, irm-^{2}H NMR has some limitations in terms of low sensitivity, restricted chemical shift range leading to signal overlap, and small dynamic range; a molecular weight above 250 g.mol^{-1} results in ^{2}H NMR spectra with low resolution due to efficient relaxation. These are not (or are only partly) compensated by using a very high magnetic field and cryoprobe, prohibiting the study of compounds found in final matrices or in environmental samples. Furthermore, the hydrogen atom (and therefore ^{2}H) is in many cases easily exchangeable. All these problems are circumvented by studying a nucleus such as ^{13}C (or even ^{15}N). The intrinsic NMR properties of ^{13}C are clearly much more favorable than those of ^{2}H, as summarized in **Table 2**.

However, the requirement for nOe suppression, combined with the long ^{13}C T_1 values, and the high signal-to-noise ratio (SNR), leads to long measurement times. Nevertheless, by using a relaxation reagent (such as tris(2,4-pentadionato)chromium(III) [CrAcac]) PSIA by irm-^{13}C NMR can be performed in a reasonable time-frame [14].

Table 2: Main properties of nuclei used in irm-NMR

	^{2}H	^{13}C	^{15}N	^{17}O
Magnetogyric ratio (10^{6} rad·s^{-1}·T^{-1})	41.066	67.262	-27.116	-36.279
Mean abundance (%)	0.02	1.08	0.37	0.04
Sensitivity / ^{1}H	1.4 10^{-6}	1.8 10^{-4}	3.8 10^{-6}	1.1 10^{-5}
Spin	1	1/2	1/2	5/2

3. High accuracy quantitative NMR

In this Section, we describe the conditions needed to reach the high accuracy required for isotopic NMR, after first defining the notions of trueness, precision and accuracy, since these words can take different meanings in different disciplines.

3.1. Trueness, precision and accuracy

In the field of isotope ratio measurement by NMR (irm-NMR), the definitions used for these three quantities are those proposed by Menditto *et al.* [32] and incorporated by the VIM (International Vocabulary of Metrology) in its third edition [33]. The reader will find a further critical overview in [34]. Precision is ‘‘the closeness of agreement between independent test results obtained under stipulated conditions’’, and therefore characterizes random errors. Trueness is ‘‘the closeness of agreement between the average value obtained from a large series of test results and an accepted reference value’’, and therefore characterizes systematic errors. Accuracy is the combined contribution of both precision and trueness.

3.2. Is NMR always quantitative?

In the NMR literature, the notion of quantitative NMR (qNMR) most often implies that the k coefficient of Eq. (3) is identical for all the positions i. However, this definition of qNMR is much too restrictive, notably because it excludes 1D and nD acquisitions performed with multi-pulse sequences. If such a constraint was applied to other analytical techniques, such as optical spectroscopies, chromatography or mass spectrometry, no quantitative measurement would be possible.

In fact, when the precision is good enough (with respect to the given objective), trueness can be reached by a calibration procedure, such as external calibration curves, or with an internal added standard [35]. Consequently, as described below, all NMR sequences can be used for quantitative analysis if they have been previously optimized in order to obtain the target repeatability.

3.3. Parameters influencing trueness

3.3.1. Partial saturation

Because of the signal-to-noise ratio (SNR) or phase cycling, multiple FIDs are usually accumulated before Fourier transform. For this purpose, the pulse sequence is repeated and a steady state is gradually established during the early scans [36]. In the case where each scan is preceded by a single RF observe pulse, the longitudinal magnetization present before the pulse reaches the equilibrium value:

$$M_{eq} = M_0.\frac{(1-\cos(\beta)).e^{-\frac{TR}{T_1}}}{1-\cos(\beta).e^{-\frac{TR}{T_1}}} \quad (5)$$

where β is the flip angle induced by the RF pulse, TR is the repetition time and T_1 is the longitudinal relaxation time [36].

The maximal amplitude for the detected signal is then obtained when β is equal to the so-called Ernst angle ($\beta_E = arcos(e^{-\frac{TR}{T_1}})$) calculated by taking the derivative of Eq. (5) [36]. It should be noted that this expression is only correct if no transverse magnetization remains before the next RF pulse; otherwise residual transverse magnetization interferes with longitudinal magnetization and contributes to the steady state.

Whatever the value of β, the T_1 values of signals from different chemical groups differ. Eq. (6) gives the percentage deviation E which characterizes the error due to partial saturation:

$$\mathrm{E} = 100.\frac{e^{-\frac{TR}{T_1}}.(1-\cos(\beta))}{1-\cos(\beta).e^{-\frac{TR}{T_1}}} \quad (6)$$

Trueness is then limited by E obtained for the longest T_1 (T_1^{max}).

For a given value of E, one obtains an infinity of couples (β, TR/T_1^{max}), corresponding to the intersection between the surface represented in **Figure 3** and a horizontal plane. Among these

couples, it is now necessary to determine which ensures the best precision. How this is done will be described in Section 3.4.

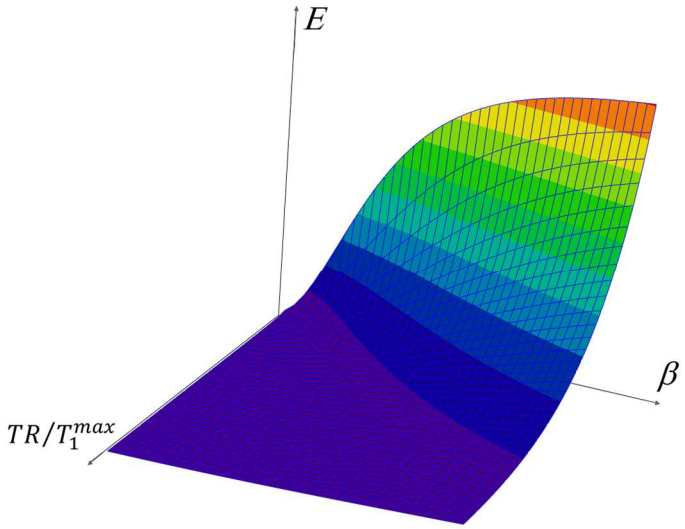

Fig. 3: Plot of the error E against the flip angle β and the ratio TR/T_1^{max}.

3.3.2. Off-resonance

In the ideal case where the radiofrequency pulse has high power, it is possible to neglect the precession around $\vec{B}_0$ during the pulse and to consider that all the magnetizations contributing to the spectrum undergo - during an RF pulse of duration τ- a rotation of angle $\beta_0 = \omega_1.\tau$. This approximation is frequently made when an accurate analysis is not necessary.

However, in many experimental situations, this approximation is not satisfied. In fact, magnetization precession takes place around an effective field which is not in the transverse plane [36]. The evolution of M_{xy}/M_0 as a function of Ω_0/ω_1 is shown in **Figure 4** for a nominal flip angle of $\pi/2$. Here, Ω_0 is the signal offset in the rotating frame. It can be seen that M_{xy} remains close to M_0 as long as Ω_0 does not exceed ω_1. For larger offsets, M_{xy} decreases rapidly and even goes through zero.

As a first approximation, the evolution of M_{xy} as a function of Ω_0 is often described by a sinc function. It is therefore reported, for comparison, in **Figure 4**.

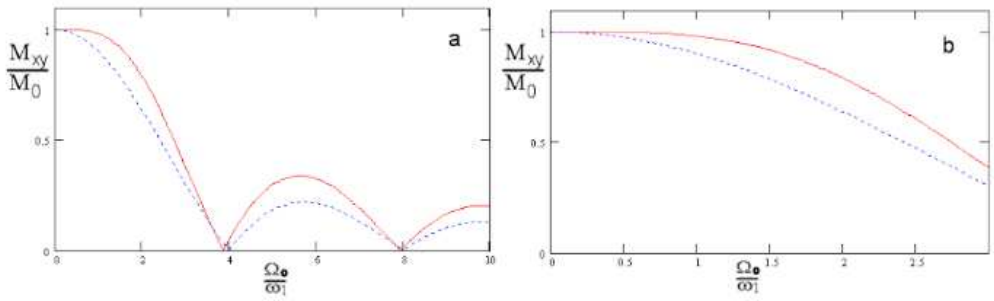

Fig. 4: Evolution of $\frac{M_{xy}}{M_0}$ with $\frac{\Omega_0}{\omega_1}$ from 0 to 10 (a) and from 0 to 3 (b). Dotted lines represent the $\sin\left(\frac{\Omega_0.\tau}{2}\right)/\left(\frac{\Omega_0.\tau}{2}\right)$ function for comparison.

This off-resonance effect is another source of error and, for a single-pulse acquisition, trueness is therefore limited by the ratio M_{xy}/M_0. Because this effect depends on resonance frequency, the greatest error is observed at the bandwidth edges. For a given error, it is thus possible to calculate the maximum permitted bandwidth ΔF^{max}. A close examination of the curve plotted in **Figure 4** shows that an error of 1% ($M_{xy}/M_0 = 0.99$) is obtained for $\Omega_0/\omega_1 = 0.84$ which corresponds to $\Delta F^{max} = 0.42/\tau_{90}$, where τ_{90} is the duration of a π/2 flip angle on resonance. An error of 1‰ ($M_{xy}/M_0 = 0.999$) is obtained for $\Omega_0/\omega_1 = O.46$ and $\Delta F^{max} = 0.23/\tau_{90}$.

3.3.3. Heteronuclear decoupling

Continuous heteronuclear irradiation, for example during heteronuclear decoupling, induces the nuclear Overhauser effect (nOe). Because this effect is not instantaneous and builds up gradually, it is possible to avoid its influence on peak areas by using inverse gated decoupling [37]. Theoretical descriptions and experimental studies indicate that a long enough repetition time can enable the full recovery of the magnetization to its initial value with no nOe [37, 38]: it has been shown that $TR = 10.T_1^{max}$ is necessary to reach an accuracy close to 1‰ [39].

As will be discussed in Section 3.5, the best results for high-accuracy quantitative NMR are obtained using lineshape fitting to determine peak areas. However, this is only true when experimental lineshapes are very close to the theoretical model used (Lorentzian, Gaussian or a combination of the two).

Line shape distortion can notably come from imperfections in heteronuclear decoupling. They can disperse signal into sidebands, causing signal loss and can leave a residual splitting which is too small to be resolved but induces deviation of the lineshape from the ideal model, reducing fitting efficiency and so decreasing trueness (**Fig. 5**) [21].

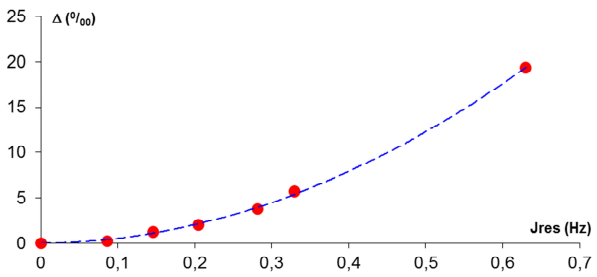

Fig. 5: Impact of the residual coupling J_{res} (resulting from imperfect ^{1}H decoupling) on the trueness of isotopic ^{13}C NMR measurements. Δ is the variation in relative intensities for ethanol. Reprinted with permission from Ref. [21]. Copyright 2017 Wiley.

Furthermore, it has been shown experimentally [40, 41] that composite pulse decoupling schemes do not allow uniform decoupling over the proton chemical range. This limits trueness to the order of a few percent.

Broadband heteronuclear decoupling has been the subject of numerous studies [42], mainly during the 1990s. However, these works essentially focused on increasing the width of the decoupled frequency range. To achieve excellent accuracy over the entire ^{13}C range, the ^{1}H decoupling must be as uniform as possible. In order to reach this goal, an original approach had to be developed: for each offset, the minimum adiabaticity factor reached during the pulse was computed, and then the profile

obtained was used to optimize the swept frequency range of the adiabatic pulses [41]. This led to adiabatic full passage pulses with a cosine amplitude modulation of the RF field (ω_2^{max} = 75.2 kHz). A frequency sweep was performed using the offset independent adiabaticity strategy [43] over an optimized bandwidth of 14 kHz and the M4P5–M4P9–M4P50–M4P90 phase cycle was used. As shown in **Figure 6**, this resulted in a dramatic improvement in proton decoupling uniformity and so in trueness.

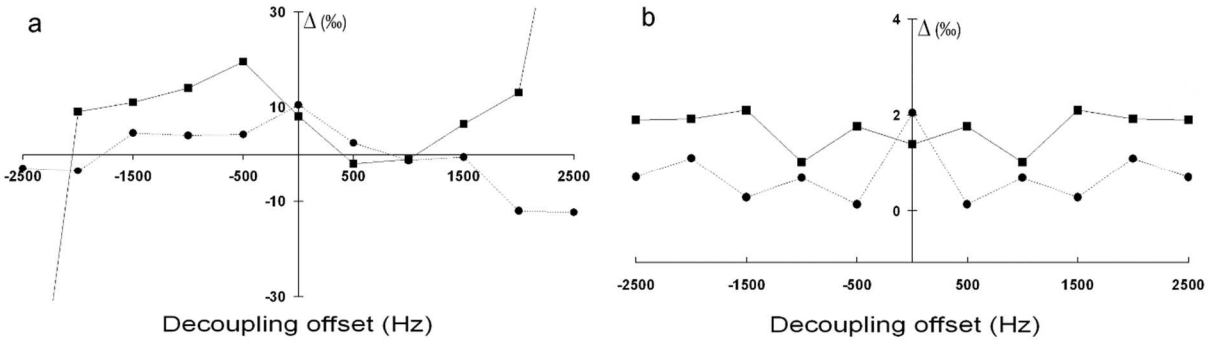

Fig. 6: Δ values (in ‰) as a function of the decoupling offset for the acetic acid molecule (···●···) and for the ethanol molecule (-■-). (a) The decoupling was performed using WALTZ-16 with ω_2^{max} = 53.1 kHz. (b) The decoupling scheme used Cos/OIA pulses with ω_2^{max} = 75.2 kHz. Note the difference in the vertical scale between (a) and (b). In this article Δ has the same meaning as Γ, defined in section 4.3.2. Reprinted with permission from Ref. [41]. Copyright 2007 Elsevier.

3.3.4. Pulse sequence

Whatever the sequence used, all the parameters mentioned previously affect trueness, and for some of them, such as resonance offset, the effect increases when multi-pulse sequences are used. Moreover, in the latter case, transverse relaxation and chemical shift and coupling effects have to be added [44].

Therefore, the signal of position i can be written:

$$S_i = k'.\lambda_s.\lambda_n.\lambda_d.\lambda_p.n_i.c.x_i \quad (7)$$

where λ_s, λ_n, λ_d, λ_r and λ_e are factors characterizing the effect of partial saturation, nOe, heteronuclear decoupling, transverse relaxation and chemical shift and decoupling changes, respectively. Clearly, this is not an exhaustive list.

3.4. Parameters influencing precision

3.4.1. Signal-to-noise ratio

The main limit on precision for NMR measurement is the SNR, which can be formalized by [45]:

$$\sigma \leq \frac{1}{2.SNR} \quad (8)$$

where σ is the relative standard deviation of the peak area.

This relation was demonstrated experimentally by Caytan *et al.* [14] for isotopic measurements (irm-^{13}C NMR) performed on vanillin samples (**Fig. 7**).

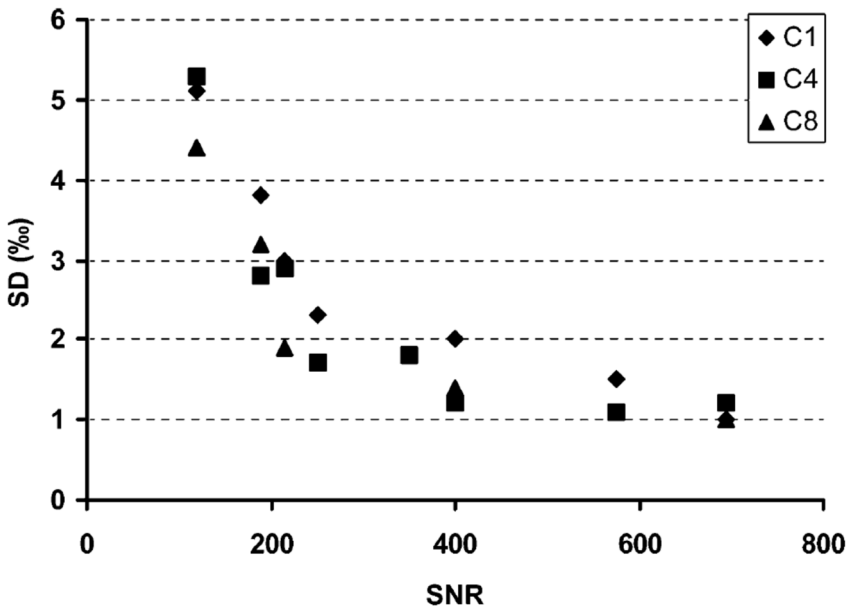

Fig. 7: Dependence of the relative standard deviation in permil (‰) on the signal-to-noise ratio (SNR) for three carbons of the vanillin molecule (see Fig. 20 carbon numbering). Reprinted with permission from Ref. [14].

Consequently, among the set of couples (β, TR/T_1^{max}) described in Section 3.3, it is necessary to determine which one ensures the best SNR for a given acquisition analysis time Ta. It is straightforward to demonstrate that:

$$SNR_{(Ta=Cte)} = k.\frac{M_{eq}.\sin(\beta)}{\sqrt{TR}} \quad (9)$$

where $SNR_{(Ta=Cte)}$ is the signal-to-noise ratio obtained in a given Ta. $SNR_{(Ta=Cte)}$ is plotted in **Figure 8** against the ratio TR/T_1^{max} and the flip angle β.

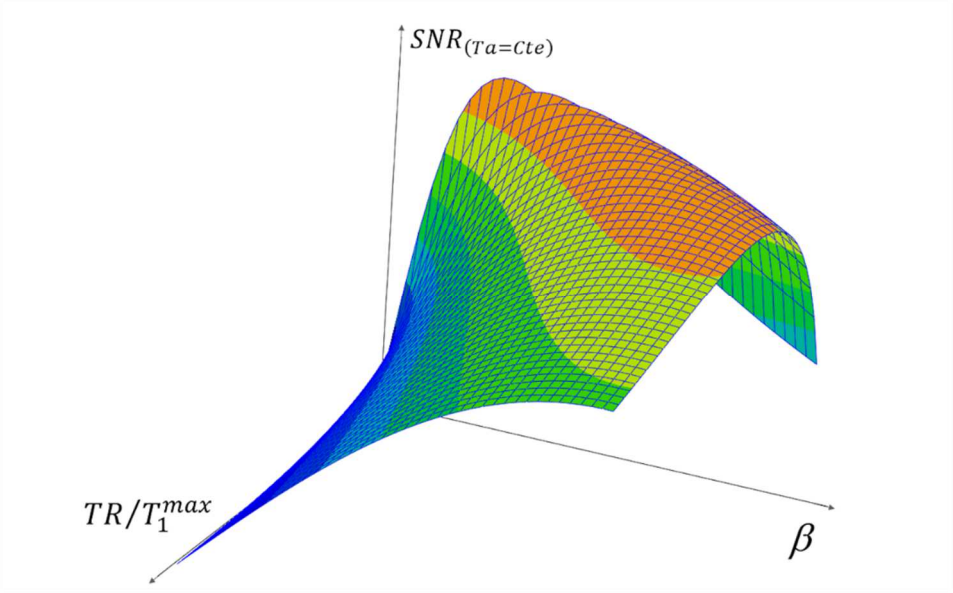

Fig. 8: Plot of the $SNR_{(Ta=Cte)}$ against the flip angle β and the ratio TR/T_1^{max}.

The intersection between the two sets of couples (β, TR/T_1^{max}) (obtained on the basis of trueness and precision) provides an optimal couple (β^{opt}, TR^{opt}/T_1^{max}).

The optimal flip angle β^{opt} and the optimal ratio TR^{opt}/T_1^{max} are plotted *versus* the targeted error due to partial saturation E in **Figure 9**. It appears that the more demanding we are of E, the closer β is to 90° [37, 38, 39].

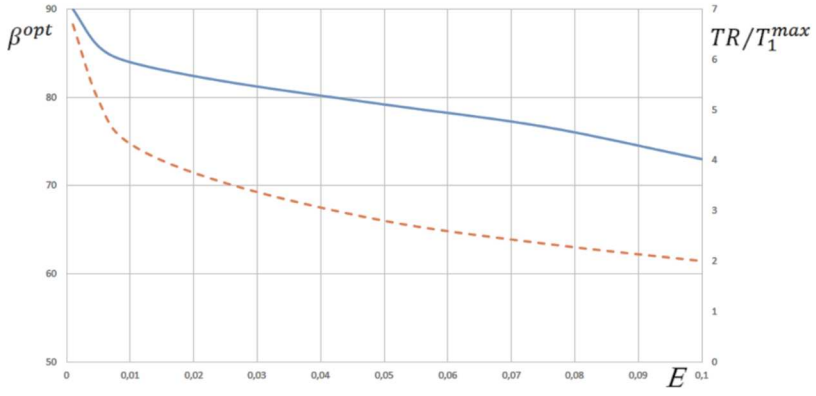

Fig. 9: Plot of the optimal flip angle β^{opt} (solid line) and the optimal ratio TR^{opt}/T_1^{max} (dashed line) against E, the target value in terms of trueness and precision.

In addition, as $\frac{\partial M_{xy}}{\partial \beta}$ is proportional to $\cos\beta$, a variation ∂β of the readout pulse produces a variation ∂M_{xy} of the magnetization proportional to $\cos\beta$. It is therefore for β close to 90° that ∂M_{xy} will be minimum and that M_{xy} will be less sensitive to some instabilities of the spectrometer. It can be concluded that β = 90° ensures maximum robustness of the acquisition.

Consequently, β^{opt} = 90° is always a good choice; this leads to TR^{opt}/T_1^{max} = 3, 4.6 and 7 for E equal to 5%, 1% and 1‰, respectively. Note that when the nOe has to be taken into account, TR^{opt}/T_1^{max} = 10 has to be chosen (see Section 3.3.3).

3.4.2. Spectrometer and sample stability

Clearly, the stability of the sample plays a big part in the precision obtained and this point has been extensively developed in the literature [46-48]. In general, the stability of all parameters influencing trueness has a significant impact on precision. This is notably the case for temperature; both that of the sample and that of the probe and electronic devices are crucial to obtaining good precision.

In addition, all these variations should not only be considered individually. A combination of several variations can impact precision more severely than the sum of the effects of each individual instability. As an example, RF pulse imperfections cause non-uniform decoupling, which decreases

trueness. However, when such imperfections are caused by temperature instability, which also induces chemical shift variation, it is responsible for the poor precision observed with classic decoupling schemes [40, 41].

3.4.3. Pulse sequence

We mentioned in Section 3.3.4 that the type of sequence influences trueness, but it also has a great impact on precision. As an example, we have observed that precision obtained with the DEPT sequence is significantly lower than that obtained with a single-pulse sequence [16, 49].

This is mainly due to RF imperfections [44]. However, not all pulses have the same effect: 90° pulse imperfections reduce all peak areas to the same extent when the off-resonance effect is small [44]. Furthermore, the signal intensity depends on $\sin\beta$ so a variation in β induces a signal variation proportional to $\cos\beta$ [44]. Therefore, the instability of such pulses has a low impact on precision.

On the other hand, 180° pulse imperfections – when they are involved in a spin-echo block – are responsible for poor refocusing and so have an effect on peak area that depends on the resonance frequency [44]. Consequently, small temperature variations – that cannot be avoided even with efficient temperature control – cause a loss in precision. This effect can be overcome by replacing hard 180° pulses by shaped pulses immune to transmitter variations (such as optimized adiabatic pulses) [16, 49] (**Fig. 10**).

It should be noted that the influence of the sequence on precision can vary greatly from one sequence to another. We have shown that DEPT reproducibility – even with adiabatic 180° pulses – is not good enough for ^{13}C isotopic NMR, while adiabatic INEPT is a powerful tool for such applications [49]. Moreover, for a sequence like HSQC, the global symmetry in the RF pulse scheme seems to induce a partial compensation for imperfections, which limits the effect on precision [50].

Lastly, relaxation must be taken into account. Multi-pulse sequences include periods of time during which transverse relaxation induces a decrease in magnetization, especially when the pulse sequence includes long delays tuned for small, long-range couplings [18]. A small variation in T_2 can therefore

generate a variation in peak areas that is not negligible when the target precision is a few permil. This imposes severe constraints on the sample preparation protocol, for example the requirement to minimize the presence of paramagnetic impurities, including O_2.

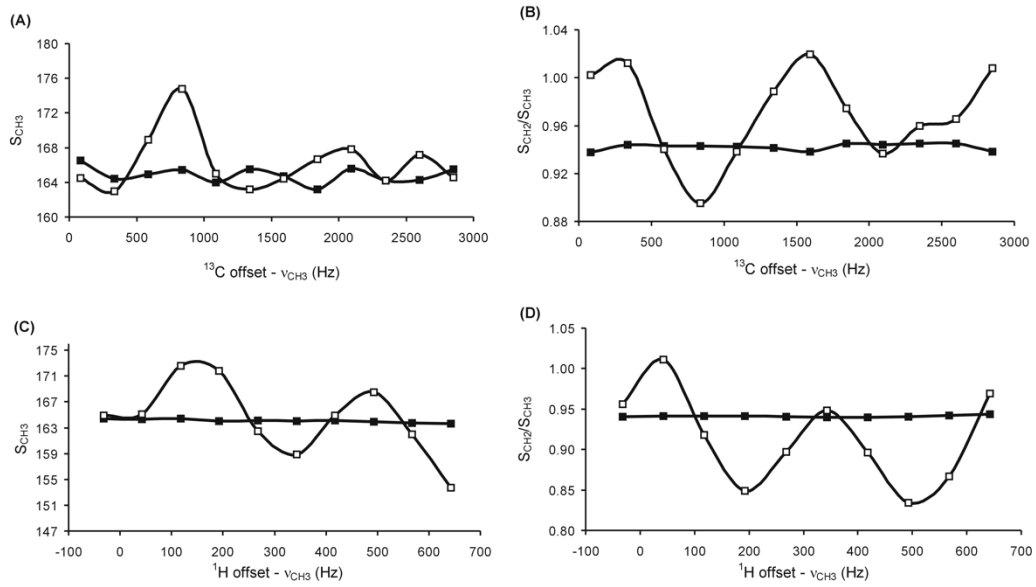

Fig. 10: Influence of ^{13}C and ^{1}H 180° RF pulse imperfections on the precision of peak areas measured with INEPT sequences. For each pulse sequence, the offset was varied systematically over 2750 Hz in steps of 250 Hz (2 ppm) for ^{13}C, and over 675 Hz, in steps of 75 Hz (0.15 ppm) for ^{1}H. Standard INEPT sequence □; adiabatic INEPT sequence with composite refocusing pulses (COS/OIA) (▪). (A) Dependence of CH_3 (S_{CH3}) ^{13}C peak areas in INEPT spectra on the difference between ^{13}C offset and chemical shifts of CH_3. (B) Ratio S_{CH2}/S_{CH3} of peak areas as a function of the difference between the ^{13}C carrier offset and the chemical shift of the CH_3 group. (C) Dependence of CH_3 (S_{CH3}) peak areas in INEPT spectra on the difference between ^{1}H offset and CH_3 chemical shift. (D) Ratio S_{CH2}/S_{CH3} of peak areas as a function of the difference between the carrier ^{1}H offset and the chemical shift of the CH_2 group. Reprinted with permission from Ref. [16]. Copyright 2007 ACS.

3.5. Experimental conditions for high accuracy quantitative NMR

From all the considerations mentioned in Section 3, we can derive optimized experimental conditions for performing high accuracy quantitative NMR at the level needed for isotopic analysis. The key points are: (i) precision is the first objective, and (ii) trueness can be reached by a calibration procedure, but only if the λ_i factors of Eq. (7) are reproducible.

In this quest for accuracy, temperature plays an important role; it must therefore be strictly controlled, particularly that of the room and of the sample. Moreover, in most cases, the sample temperature before it is introduced into the probe differs from the working temperature. Consequently, there must be a significant stabilization time between sample introduction and the first instrumental adjustments (probe tuning and matching) [48], in order to ensure that the temperature is completely stable and homogeneous. As an example, 15 minutes is a minimum stabilization time for a 5 mm tube introduced at room temperature into a probe regulated at 303 K and for a sample in water. This time increases with the temperature difference and the tube diameter and it also depends on what solvent is used.

Concerning the influence of longitudinal relaxation and nOe, they depend strongly on both temperature and the presence of paramagnetic impurities. Then, it is very difficult to obtain reproducible values for factors λ_s and λ_n. Therefore, it is essential to eliminate these two contributions to inaccuracy, as described in Sections 3.3.3 and 3.4.1 [13].

As described in Sections 3.3.3 and 3.4.2, high accuracy implies an optimized adiabatic decoupling. However, the decoupling conditions described in Section 3.3.3 lead to high RF energy deposition [41]. A sampling time of 1 second is thus a good compromise between FID truncation and hardware and sample safety. Furthermore, the probe geometry is an important parameter for efficient decoupling. Inverse probes must not be used for X-nucleus acquisition since the proton coil, located as closely as possible to the sample, is shorter than the X (^{13}C, ^{15}N or ^{17}O) coil. In such a configuration, some of the X nuclei are not correctly decoupled, which induces distortions in lineshape [51].

Multi-pulse sequences can be used and they are a good choice to improve the SNR [16, 49, 50, 52]. However, the type of 180° RF pulses must be carefully chosen and, once again, adiabatic pulses are a good solution [16, 49]. DEPT must be avoided since it includes an RF pulse that is neither 90° nor 180° – at least if all the carbons bearing proton(s) are measured.

562 Finally, data processing, especially the method used to determine peak areas, is crucial to reach high
563 accuracy. In the absence of significant signal overlap, integration is the most common approach to
564 determining peak areas. However, in practice, it often underestimates the areas because of
565 truncation of the long tails of the Lorentzian lineshape [53]. One of the more important criteria when
566 choosing the method to measure peak areas is that it must be as independent as possible of the
567 operator. From this point of view, the best solution is to perform a fit of the experimental data with a
568 theoretical model (*e.g.* Lorentz-Gauss), which must take many parameters into account so that the
569 areas under the peaks are determined with great precision. This adjustment must be made at least
570 on the position, width and intensity, but this is generally not enough to reach a few permil [31]. Shim
571 imperfections generate broadening and distortions in lineshape. A contribution of Gaussian and
572 asymmetry must therefore be incorporated into the model. Asymmetry in lineshape is allowed for by
573 introducing a term in the first derivative of the Gaussian contribution into the lineshape model [54].
574 From our experience, an error of only 5% in the Gaussian percentage can induce a bias of 10% in the
575 area determined. Taking into account the peak phases is also crucial since it is impossible to phase
576 heteronuclear spectra perfectly with a correction of order one. We have found that a four-degree
577 phase shift (invisible to the naked eye) causes a few permil error in the peak area. In addition, the
578 baseline must be corrected very carefully, which is difficult to do on the complete spectrum. The best
579 option is to integrate it into the line-fitting, which must thus be adjusted for each line: position,
580 width, intensity, phase, Gaussian %, asymmetry and baseline [31, 55]. This adjustment can be made
581 in the time domain or in the frequency domain.

582

4. Isotope ratio measurement by NMR

4.1. Isotopic fingerprinting

The determination of molar fractions f_i using Eq. (4) is sufficient to measure the relative contents of the different isotopomers if it is carried out with high precision (% for ^{2}H and ‰ for ^{13}C or ^{15}N). For authentication applications, trueness is not an issue and the molar fraction profile is thus sufficient to obtain an isotopic fingerprint. Moreover, in such cases, it is not always essential to measure the isotope content of all the positions [56] and intensity distortions induced by multi-pulse sequences are not drawbacks [49, 57], even in 2D [50, 52] (see Section 5). As an example, in the case of the INEPT sequence, the transfer of polarization leads to an increase in sensitivity up to a factor of four and a gain is also achieved by shortening the TR, since it is now governed by the ^{1}H T_1 values, which are significantly smaller than those of ^{13}C. TR can be set at the value of seven times the proton T_1^{max}, which contributes to decreasing the analysis duration.

4.2. Position-specific isotope abundance measurement

As mentioned in the previous Section, molar fractions f_i only give the relative contents of the different isotopomers. Two methods can be used to obtain absolute position-specific isotope abundances (x_i).

4.2.1 Using average isotope abundance

If the average isotope abundance of the entire molecule (x_g) is known, specific isotope abundances (x_i) can be calculated using Eq. (10).

$$x_i = x_g . \frac{f_i}{F_i} \qquad (10)$$

where F_i is the statistical molar fraction (*i.e.* without any isotope fractionation); $F_i = n_i / \sum n_i$ with n_i the number of equivalent nuclei at the position i.

x_g is determined using irm-MS, so this method requires the use of two different analytical techniques: NMR and mass spectrometry. Furthermore, it can only be used when the molar fractions of all sites are measured [31].

4.2.2. Using an isotopic internal reference

The $\boldsymbol{x_i}$ values can also be obtained by using an internal reference of known isotope abundance [58].

$$x_i = x_{ref} \cdot \frac{S_i}{S_{ref}} \cdot \frac{n_{ref}}{n_i} \cdot \frac{c_{ref}}{c} \quad (11)$$

where x_{ref} is the isotope abundance of the reference compound; S_{ref} is the peak area of the reference compound; n_{ref} is the number of equivalent hydrogens associated with the reference; C is the molar concentration of the measured compound and C_{ref} the molar concentration of the reference compound.

The basic way to determine the molar ratio C_{ref}/C is to use gravimetry:

$$\frac{c_{ref}}{c} = \frac{m^{ref} \cdot P_m^{ref}}{m \cdot P_m} \cdot \frac{M}{M^{ref}} \quad (12)$$

Here, m and M are the weights used for the NMR tube preparation and the molar mass, respectively, and p_m is the mass purity.

This approach is effective for ^{2}H because the required precision is only of the order of a percent, but it turns out to be extremely delicate for ^{13}C or ^{15}N because the precision is then of the order of a few permil.

The second way to determine the molar ratio is to use ^{1}H NMR [59].

$$\frac{c_{ref}}{c} = \frac{S_{1_H}^{ref} \cdot n_{H_i}}{S_{1_{H_i}} \cdot n_H^{ref}} \quad (13)$$

With this approach, all the data are obtained with NMR without need of another method. Moreover, if there are no overlaps between the signals being analyzed and signals from any impurities that may be present, then it is no longer necessary to know purities. In addition, it is no longer essential to measure all the sites and thus multi-pulse sequences can be used as long as specific factors (λ_i) are

determined by comparison with data from single-pulse acquisitions (this last point is currently being validated in our laboratory).

However, to measure ^{13}C NMR spectra with high precision, a high SNR and thus high concentrations are necessary. If the proton spectrum is acquired from the same sample as for the ^{13}C spectrum, the former may be corrupted by radiation damping, which is incompatible with high accuracy measurement.

This last drawback can be overcome by specific methods. We have shown that accurate ^{1}H quantitative NMR can be performed on concentrated samples by suppressing most of the signal and keeping only that coming from a thin slice in the center of the sample [60, 61].

4.2.3. Correction for contribution of bi-labeled isotopologues

Before applying Eqs. (10) or (11) to calculate isotope abundances, peak areas must be corrected to take into account the contribution of bi-labeled isotopologues [62]. This can be disregarded for ^{2}H because of its low natural abundance, but not for ^{13}C. The isotopologues bearing a ^{13}C at position i include mono-labeled isotopologues (one ^{13}C at position i and only ^{12}C at other positions) and multi-labeled isotopologues (one ^{13}C at position i and ^{13}C at other positions). Isotopologues with more than two ^{13}C are too scarce to make a significant contribution, but bi-labeled isotopologues generate doublets (satellite lines). When the two ^{13}C are separated by at least two bonds, satellites are included in the peak tails and these isotopologues contribute to the area of the main line (see **Fig. 2**). However, when the two ^{13}C are at adjacent positions, the satellite lines are well resolved because the ^{13}C-^{13}C scalar coupling values are large. Because of their SNR, it is not possible to quantify these satellite lines with high accuracy, but they can be taken into account using Eq. (14).

$$S_i = S'_i\,(1 + u \times 0.011) \qquad (14)$$

Here, S'_i is the area under the main peak, u is the number of carbons linked to position i, 0.011 is the average natural isotope abundance of ^{13}C and S_i is therefore proportional to the total number of ^{13}C located at position i.

4.2.4. Partial, apparent and true isotopic composition

The isotopic compositions measured by the single-pulse methodology (with inverse gated adiabatic decoupling) are expected to be the "true" values. This is almost always the case for standard NMR spectrometers, as shown by the ring test performed on similar instrumental configurations (400 MHz and BB or dual $^{13}C/^{1}H$ probes) from which an inter-machine standard deviation lower than 2‰ was found [51]. Furthermore, the $\delta^{13}C_i$ values were very similar to those found by other PSIA methods such as pyrolysis coupled to irm-MS [63]. Nonetheless, significant variations were found in relation to the range of the chemical shifts: the extreme side peaks of the spectrum showed the largest discrepancies [64]. This divergence is accentuated by using cryoprobes at very high fields. "True" values would be obtained by applying correction factors, depending on the spectrometer response after measuring international standards, from which a consensus on the intramolecular ^{13}C distribution could be established. Work is in progress to select molecules, such as alanine [65], that could fit these requirements.

When multi-pulse sequences such as INEPT are used, polarization transfer is commonly achieved using $^{1}J_{13C\text{-}1H}$ couplings. As a result, the quaternary carbons are not observed. The ^{13}C profile is therefore partial. In addition, the intensity of the signal is affected by the values of transfer and refocusing delays, that is to say that the λ coefficients of Eq. (7) are not the same for all the detected peaks. Areas are not solely proportional to the number of nuclei but also depend on the sequence parameters. Therefore, the measured f_i values are partial and apparent as they are not the true molar fractions of all isotopomers. The only parameters that can provide a full statistical distribution are therefore these partial fractions f_i or f_i / F_i. When the number of quaternary carbons is relatively small compared to the protonated carbons, the partial profile, *i.e.* with the protonated carbons only, is usually enough for effective discrimination between samples. The resulting partial intramolecular distribution leads to profiles that could be used as input data for -omics interpretation (isotopomics). The calculation of the position-specific ^{13}C isotope composition $\delta^{13}C_i$ cannot be performed as is done

679 for the single-pulse experiment, for which the full ^{13}C distribution can be retrieved relatively from the
680 global ^{13}C content (measured by irm-MS, for example, see Section 4.2.1) once all area signals have
681 been deconvoluted. Eq. (10) cannot be used because it requires all the peaks to be measured. The
682 conversion to $\delta^{13}C_i$ would be possible from the internal reference by calculating the apparent isotopic
683 composition of the available isotopomers. As discussed above, correction factors could then be
684 applied to express these $\delta^{13}C_i$ on a consensual international δ-scale.

685 In some cases, the number of quaternary carbons is not negligible and information is missing, as
686 illustrated by the study of the origin of caffeine (see Section 5). The delay for the transfer of
687 polarization in INEPT can be adjusted to the long-range ^{1}H-^{13}C couplings ($^{n}J_{13C\text{-}1H}$). However,
688 adaptations were required in order to reach the targeted precision, and matched transfer and
689 refocusing delays were found [18]. $|^{n}J_{13C\text{-}1H}|$ can range from 0 to 20 Hz, leading to spin-echo periods
690 longer than 100 ms in total. The loss of signal via transverse relaxation cannot be neglected: one has
691 to be sure that the signal attenuation caused is always the same, whatever the sample or the
692 experiment, for a given molecule. Robustness is ensured by fixing the acquisition parameters and the
693 sample preparation. The resulting methodology was named Full-Spectrum INEPT (FS-INEPT) [18]. It
694 was shown that the full ^{13}C profiles could be obtained with 40 mg of caffeine or acetaminophen in a
695 short time (see Section 5). This strategy was also tested for ^{15}N profiling, since several (bio)organic
696 nitrogen-containing molecules do not exhibit $^{1}J_{15N\text{-}1H}$ couplings, providing long-range couplings only.
697 In these cases, all the peaks are measured and apparent isotope compositions are obtained once
698 again [19]. Eq. (11) leads to apparent isotope compositions $\delta^{13}C_i$ or $\delta^{15}N_i$ that are meaningless, *i.e*. are
699 not expressed on the absolute scale from the international standard V-PDB for ^{13}C or from
700 atmospheric N_2 for ^{15}N, as obtained by irm-MS ($\delta^{13}C_g$ and $\delta^{15}N_g$) or even from an internal reference.
701 As mentioned above, to retrieve the true isotopic compositions, appropriate calibration has to be
702 performed, by comparing the values obtained on a reference sample of the given molecule with the
703 single-pulse sequence and with the multi-pulse sequence, leading to suitable correction factors.
704 However, even when only apparent isotope compositions are obtained, the variations between

samples are on the same scale as irm-MS: if $\Delta\delta_i$ is defined as the change in isotopic composition between samples, it is then as correct as $\Delta\delta g$ (obtained by irm-MS) even if δ_i is not on the standardized scale. The extent of $\Delta\delta_i$ can be directly compared to $\Delta\delta_g$ since they are expressed on the same relative scale with similar precision.

4.3. Practical aspects

4.3.1. T_1^{max} measurement

As discussed in Section 3, knowledge of the greatest longitudinal relaxation time ($\boldsymbol{T_1^{max}}$) is necessary to establish optimal conditions for high accuracy NMR.

Saito *et al.* [45] showed that the target accuracy for the area determination (ξ_S) is linked to the accuracy of the T_1^{max} determination (ξ_{T_1}) by Eq. (15).

$$\xi_S = \sqrt{\left(\frac{\partial S}{\partial T_1}\right)^2 . \xi_{T_1}^2} \quad (15)$$

which means that, whatever the $\boldsymbol{\xi_S}$ value, 10% is sufficient for $\boldsymbol{\xi_{T_1}}$ [45].

In order to obtain the best dynamic range, the inversion-recovery sequence must be used with the first inversion time (TI) close to zero and the last TI equal to five times the expected value for T_1^{max} [66].

Regarding the values and distribution of TI, we have evaluated three strategies. Montecarlo simulations were done using 4, 6, 8 and 16 values of TI ranging from 5 ms to $5.T_1^{max}$ and distributed following an arithmetic progression, a geometric progression, or a distribution assuring the arithmetic progression of M_z (Eq. (16)).

$$TI_k = -T_1^{expt} . Ln\left(1 - \frac{k}{N}\right) \quad (16)$$

where N is the number of TI values, T_1^{expt} is the expected value for T_1^{max}, and k ranges from 0 to N. The *TI* value giving $M_z = 0$ is omitted.

727 This last strategy with $N = 6$ gives the best accuracy for T_1 when simulations are performed at a
728 constant SNR and constant experimental time.

729

730 **4.3.2. Spectrometer performance evaluation**

731 The success of high accuracy quantitative NMR is greatly dependent on hardware specifications and
732 stability. It is therefore essential to evaluate the spectrometer performance in terms of trueness and
733 precision on a standard sample. However, it is not easy to obtain a sample with several chemical
734 shifts and known specific natural isotope abundances, since NMR is the only method that can
735 measure this. To address this problem, we have proposed using bi-labeled two-carbon molecules
736 such as ^{13}C-1,2-ethanol or ^{13}C-1,2-acetic acid [13, 40].

737 **Figure 11** shows the ^{13}C NMR spectrum of ^{13}C bi-labeled ethanol. The $^{13}CH_3{}^{13}CH_2OH$ isotopologue
738 gives rise to two doublets, due to ^{13}C-^{13}C scalar coupling, while the $^{12}CH_3{}^{13}CH_2OH$ and $^{13}CH_3{}^{12}CH_2OH$
739 isotopologues generate one singlet each. There is no overlapping of these six lines and so it is easy to
740 quantify the peaks of the bi-labeled isotopologue without interferences.

741 This isotopologue plays the role of the standard molecule. In the absence of instrumental
742 imperfections, the areas of the two doublets are identical, regardless of the real ^{13}C abundance of
743 each site of bi-labeled ethanol. Thus, the ratio of the $^{13}CH_2$ doublet area to the $^{13}CH_3$ doublet area is
744 exactly equal to 1.000. This can be evaluated experimentally using the parameter $\Gamma\ (‰)$ defined by
745 Eq. (17) [13].

746 $$\Gamma\ (‰) = \left(\frac{f_{CH2}}{F_{CH2}} - 1\right) \times 1000 = \left(\frac{f_{CH2}}{0.5} - 1\right) \times 1000 \qquad (17)$$

747

748 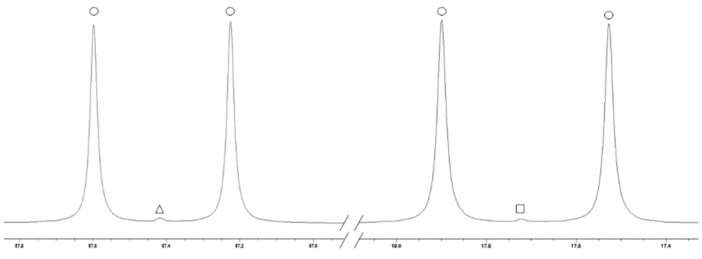

749 **Fig. 11:** Proton decoupled ^{13}C NMR spectrum of ^{13}C bi-labeled ethanol. (○) Peaks due to the $^{13}CH_3{}^{13}CH_2OH$
750 isotopologue, (Δ) peak due to the $^{12}CH_3{}^{13}CH_2OH$ isotopologue and (□) peak due to the $^{13}CH_3{}^{12}CH_2OH$
751 isotopologue.

752 ^{13}C-1,2-ethanol and ^{13}C-1,2-acetic acid are commercially available and are each of interest for specific
753 reasons. Acetic acid is used to evaluate the impact of a broad ^{13}C chemical range, and ethanol to take
754 into account the impact of proton-proton homonuclear scalar coupling. Studies with these two
755 molecules have established the experimental conditions required to obtain the high trueness and
756 precision needed by irm-NMR [13, 14, 41]. They are also an essential element in evaluating a
757 spectrometer before using it for isotopic NMR [51].

758

5. Applications

There are many varied fields in which the isotope ratios for ^{13}C or ^{15}N are used: ecology, archeology, planetology, geosciences, forensic research, metabolism, environment/climate change and authenticity/counterfeiting, to name the major applications. The previous Sections described how to perform irm-NMR and obtain the precision required. In this Section, we present typical and relevant applications of irm-NMR, mainly using ^{13}C in three areas: detection of counterfeiting, forensic investigations, and authenticity in food. The reader will find other specific contributions in the relevant literature ([67-69] for example). Finally, new applications have been found in -omics approaches. We begin with a paragraph on sample preparation, the goal of which is not to describe the specific procedure that can be found in each cited reference, but rather to focus on the general nature of the sample introduced into the NMR tube.

5.1. Sample preparation

We believe that the analyst should take care not only of the NMR parameters, as described above, but also of the sample that will be introduced into the NMR tube. The extraction and purification of the molecule to be studied must retain the isotopic integrity as it was in the matrix. Some typical preparation steps have been identified as potential sources of fractionation, while others can be used safely. We focus on the main ones, such as distillation and chromatography, as well as on derivatization. It is worth noting that intramolecular isotopic determination by irm-NMR reveals effects that irm-MS cannot detect. As such, the examples described below contribute to illustrating the interest of irm-NMR.

5.1.1. Distillation

During the liquid-vapor transition, molecules remaining in the liquid phase undergo a ^{13}C depletion as the distillate is ^{13}C-enriched, while it is the opposite for ^{2}H and ^{18}O (the light isotopologue distills first), as shown by irm-MS [70]. PSIA by irm-^{13}C NMR reveals a clear trend between the ^{13}C enrichment factors of the carbon bearing the heteroatom of chemical functions, upon distillation

784 [71]. The enrichment/depletion is strongly linked to the relative permittivity, the solvent hydrogen-
785 bond acidity, and the solvent hydrogen-bond basicity [72]. If the recovering ratio of the target
786 molecule is relatively low, the isotope fractionation could be significant, with an isotope profile that
787 would depend on the fraction collected, *e.g.* the product of interest is in the distillate or remains in
788 the tail.

789 **5.1.2. Chromatography**

790 During elution on silica gel (normal phase) as the stationary phase, the first fraction collected shows a
791 globally impoverished heavy isotope content, as found for ^{2}H, ^{13}C and ^{18}O of vanillin during the
792 purification step [73]. Furthermore, the position-specific isotope compositions show a dependence
793 on the position and functionality of the substituents present. Such non-covalent isotope effects are
794 hidden when only the global ^{13}C content is measured by mass spectrometry since they can be normal
795 or inverse and vary with the substitution pattern present, as illustrated by **Figure 12** [73].

796

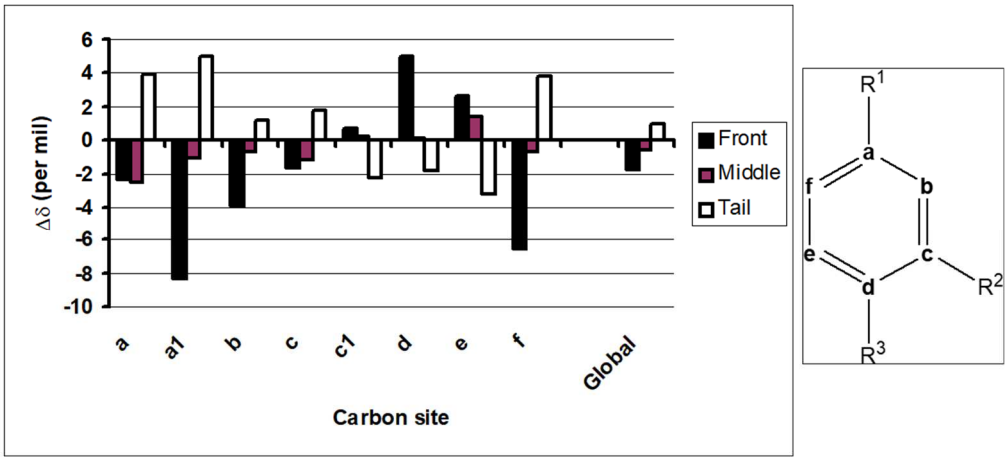

797

798 **Figure 12**: Position-specific fractionation of ^{13}C of vanillin during normal phase silica gel column
799 chromatography determined by irm-^{13}C NMR. The relative variation in $^{13}C/^{12}C$ is expressed as
800 $\Delta\delta_i = (\delta_{eluted} - \delta_{initial})_i$ for each carbon position i of the eluted vanillin $(\delta_{eluted})i$ with respect to the initial value
801 measured for site i $(\delta_{initial})i$. The numbering of each isotopomer for vanillin is for R1 = CHO, a1, R2 = OCH_3, c1
802 and R3 = OH. The data presented are from the first collected fraction (from 0 to 11%), the middle fraction (from

28 to 33%) and the last eluted fraction (tail = from 76 to 100%). Global is the total ^{13}C mean value for each of these portions determined by irm-MS. Adapted from [73].

This step is therefore a source of isotope fractionation that can be minimized via a high recovery yield (> 90%), and evaluated by determining the fractionation on the working standard on which the protocol was developed [74].

5.1.3. Miscellaneous

Extraction is often the first step required to purify the molecule of interest, by two main ways, distillation and preparative chromatography. It has been shown that both solid-liquid and liquid-liquid extraction, as well as recrystallization, do not generate isotope fractionation [74, 75]. Irm-NMR encounters the problems found in any analytical method *i.e.* the fact that analyte molecules may in general have non-ideal solubility, stability or overlapping signals. In this case, derivatization is often the preferred solution. Once again, great care should be taken to ensure the conversion yield is > 90%, to avoid significant isotope fractionation. Derivatization must be shown to lead to no, or at least a reproducible, isotope effect. As an illustration, this was well demonstrated in the study of glucose and fructose [76] and of xanthines [77] (see Section 5.4.1). Generally speaking, these purification steps should always be included in the validation of the method, in order to confirm that the isotope profile is relevant for interpretation.

5.2. Counterfeiting

The word “counterfeit” is now usually defined by and associated with the protection of intellectual property rights. On 29 May 2017, at the Seventieth World Health Assembly [78], a decision was made to adopt the term “Substandard and Falsified (SF) medical products”. The WHO proposed that “in the context of medical products, the term “falsified” appears to adequately include all the various types of deliberate misrepresentation of a medical product in such a way which enables the specific exclusion of intellectual property rights”. Testing how an active molecule was made can be useful for detecting sophisticated fraudulent practices such as (i) deliberate copying of existing patents for

828 processes or formulations; (ii) stolen and relabeled drugs; and (iii) trans-shipment of goods. Isotopic
829 approaches are the most efficient because the molecule itself is the object of the study. Classic
830 analytical tools (chromatography, mass spectrometry, *etc.*) can be used to detect the chemical
831 impurities generated from the synthesis processes used, such as the remaining raw materials,
832 intermediates and residual solvents [79]. Nonetheless, these have their limitations. Irm-MS was the
833 first isotopic method employed and was found to be particularly valuable for distinguishing batches
834 [80]. However, there is only one parameter per element (δ_g). Thus, even if a multi-element study is
835 undertaken, the number of parameters that can be used to discriminate between batches or origins
836 is still restricted to five for the common isotopes (^{2}H, ^{13}C, ^{15}N, ^{18}O, ^{34}S), depending on the atomic
837 composition [81]. In contrast, irm-NMR will provide as many parameters as isotopomers detected,
838 *e.g.* 10 parameters for a molecule containing 10 carbons by irm-^{13}C NMR, thus creating a unique tag
839 [82]. We describe here the application of irm-NMR to several APIs, highlighting the different
840 methodologies that can be used according to the type of API.

841 Twenty samples of aspirin and sixteen samples of acetaminophen were bought from pharmacies in
842 several countries and then submitted to irm-^{13}C NMR after purification of the active molecules [83].
843 Nine ^{13}C isotopomers can be observed for acetylsalicylic, acid corresponding to the nine different
844 carbons of the molecule (**Fig. 13**), and six ^{13}C isotopomers can be observed for the eight carbons in
845 acetaminophen due to the symmetry of the aromatic ring (**Fig. 13**). The single-pulse method was
846 applied, leading to ^{13}C NMR spectra with all peaks sufficiently resolved for adequate area
847 measurement. The position-specific ^{13}C composition values -notably in the substituent groups-
848 exhibit significant inter-sample variations. The origin of the acetate/acetic acid used (biological or
849 fossil) displays a large variation for both positions (C1 and C9 for acetylsalicylic acid; C1 and C6 for
850 acetaminophen), within the range usually observed for acetic acid synthesized from natural gas and
851 petrochemical sources on one hand and from a biological source, *e.g.* vinegar, on the other hand. As
852 a non-predictive tool, principal component analysis (PCA) is well adapted for studying data obtained
853 from a relatively small number of samples with a relatively large number of variables (at least > 3).

For both aspirin and acetaminophen, each sample has its own position in a 2D PCA plot (PC1 *versus* PC2), illustrating that the ^{13}C profile is unique for each product [83]. It is also clear that proximity between samples indicates that they are from similar origins.

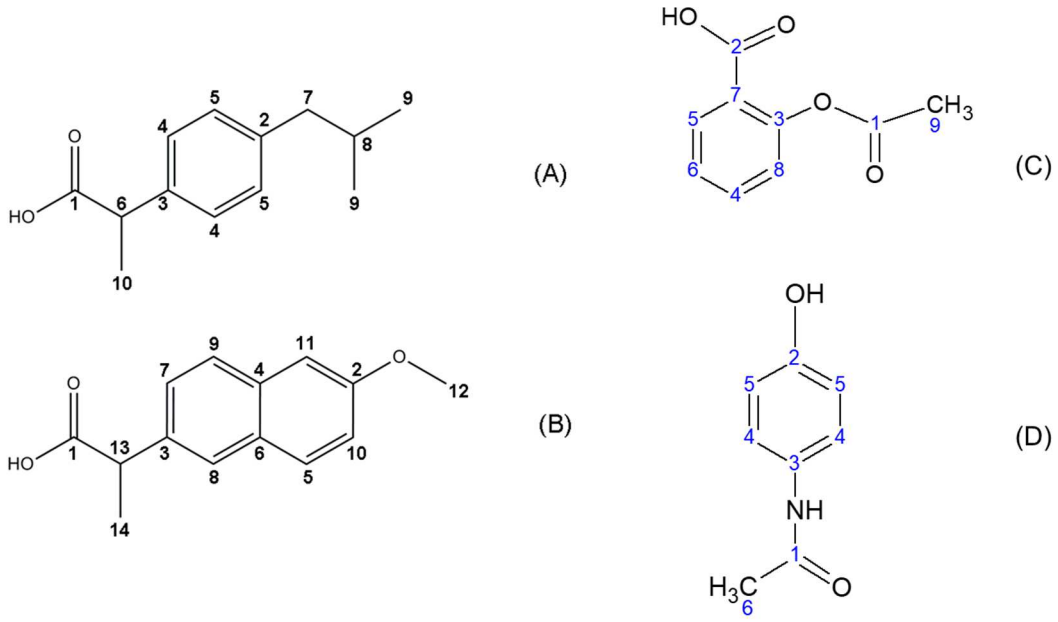

Figure 13: Molecular structure of ibuprofen (A), naproxen (B), acetylsalicylic acid (C) and acetaminophen (D) with the carbon atoms numbered in relation to the decreasing ^{13}C chemical shift in the ^{13}C NMR spectrum. This numbering is very convenient to identify easily each isotopomer from its chemical shift according to its electronic environment. In order to help readers that are not familiar to this notation, the numbered structure is linked to each NMR spectrum in the following.

The intrinsically low sensitivity of single-pulse ^{13}C NMR is still an issue for larger or less soluble molecules, as illustrated for ibuprofen and naproxen [84]. The irm-^{13}C INEPT NMR spectra of ibuprofen and naproxen were obtained in a short time. As the polarization transfer occurs via the one-bond coupling $^{1}J_{13C\text{-}1H}$, the quaternary carbons are missing. In this work, 11 samples of naproxen and 20 samples of ibuprofen were collected [84]. As discussed previously, ^{2}H NMR experiments on naproxen do not lead to useful data, even when the naproxen is esterified [85]. The global value $\delta^{13}C_g$

for both products spans a range with no clear clusters. The isotopic INEPT experiment introduces nine new parameters (f_i/F_i) for naproxen and seven for ibuprofen (**Fig. 13**).

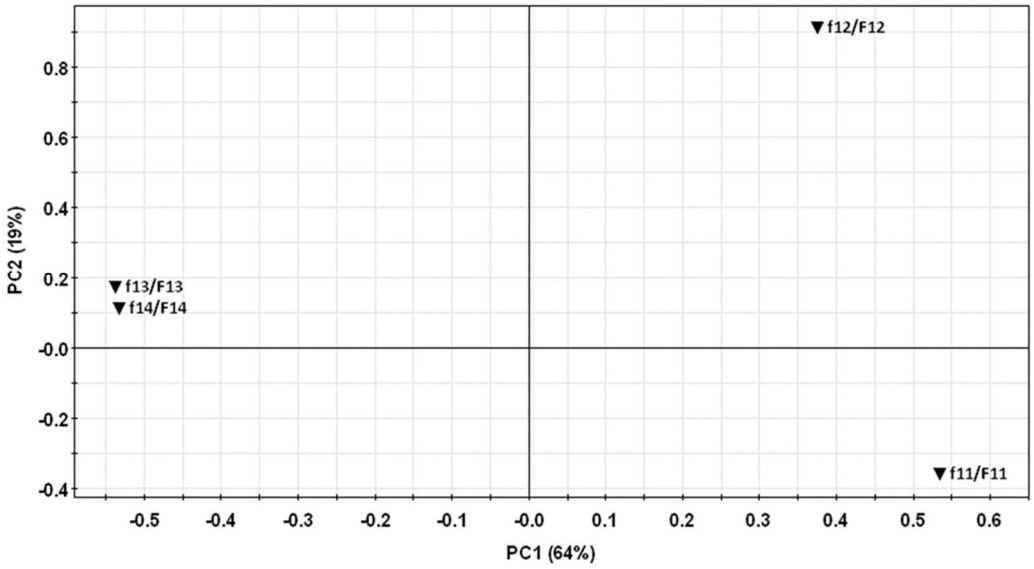

Figure 14: Loading plots from the PC1 *vs*. PC2 principal component analysis on naproxen with experimental parameters used for classification: f_{11}/F_{11}, f_{12}/F_{12}, f_{13}/F_{13} and f_{14}/F_{14} (see Fig 13 for carbon numbering).The further the parameter is located from the center, the more it contributes to the discrimination (based on data from [84]).

These factors are the apparent-partial-reduced molar fractions (see Section 4.2). 'Apparent' because the area of the signal is dependent on the delays of the INEPT sequence (but repeatable, once chosen) and 'partial' because the quaternary carbons are not observed. These factors are meaningless in themselves but their variations between samples are solely due to the change in ^{13}C distribution within the molecule that is the target of the discrimination study. For an expression of the results on the δ-scale from international standards, a correction could be applied by studying a product with a known $\delta^{13}C_i$. This stage is not beneficial for detecting counterfeiting: in fact, f_i/F_i can be used in a chemometric analysis, leading to an -omics approach (isotopomics concept). A PCA using these parameters confirms that each sample is distinguished: the individual ^{13}C profile is a marker of

889 the label origin for each batch (raw material and process). For naproxen, the explained variance of
890 77% is rather good, indicating that most of the parameters have a discrimination potential. A close
891 inspection of the data shows that the apparent-partial-reduced molar fractions f_{11}/F_{11}, f_{12}/F_{12}, f_{13}/F_{13}
892 and f_{14}/F_{14} provide the best discrimination (**Fig. 14**). Interestingly, the corresponding carbons are
893 those most involved in or closest to the reaction sites during synthesis [84].

894 ***5.3. Forensic investigations***

895 Stable isotope analyses are now an established addition to the set of forensic technologies, as they
896 can distinguish chemically identical compounds from different sources [86]. The origin of a
897 contaminant (*e.g.* during a pollution event) or sensitive materials (such as explosives) or drugs is of
898 great interest to law enforcement agencies. Isotopic profiles provide a great deal of information at
899 both strategic and tactical levels. Strategic, because often too little is known of the sources and
900 migration paths of these products. A better understanding of their marketing structure will help
901 tackle smuggling networks and hence improve global security. Tactical, because evidence that several
902 samples seized in different locations are definitely from a common origin is very valuable information
903 for field investigators and justice officers. Forensic laboratories are often asked to provide scientific
904 support for an alleged link between physical evidence and a suspect or provider. In this context, the
905 higher the number of parameters collected, the more useful the information is likely to be for
906 forensic investigations. As illustrations of the important contribution of irm-NMR to this field, three
907 examples are detailed below.

908 **5.3.1. Pollution**

909 Just after a pollution event, a forensic enquiry asks the questions: (i) Does the sample from a polluted
910 site really originate from the suspected source? (ii) How similar or different are the samples taken?
911 (iii) To what extent can we predict changes between the sample taken in the field and that from the
912 suspected source based on modelling studies of isotopic fractionation following modifying processes

(physical, chemical and biochemical remediation)? The inference of the source for determining the liable party is the main point that should be convincing for the judge.

The intramolecular ^{13}C profiles of a number of molecules well-known as pollutants – MTBE (methyl *tert*-butyl ether), ETBE (ethyl *tert*-butyl ether), TAME (*tert*-amyl methyl ether), TCE (trichloroethene), n-heptane, toluene and acetone – have been determined [87]. By comparing several origins (manufacturers), it was shown that isotope profiling of the core of a molecule reveals both the raw materials and the processes used in its manufacture. An interesting case was discussed in reference [87] concerning acetone.

Table 3: Global ^{13}C isotopic composition ($\delta^{13}C_g$) and position-specific isotope composition of the carbonyl group ($\delta^{13}C_{C=O}$) and the methyl moiety ($\delta^{13}C_{CH3}$) in ‰ of three acetone samples from several commercial batches.

Sample code	Provider	**$\delta^{13}C_g$ (‰)**	**$\delta^{13}C_{C=O}$ (‰)**	**$\delta^{13}C_{CH3}$ (‰)**
A1	Sigma-Aldrich (Batch N° 1)	-30.6	-12.8	-39.4
A2	Sigma-Aldrich (Batch N° 2)	-24.7	-7.3	-33.4
A3	Junsei Chemical	-6.4	12.7	-16.0

Table 3 summarizes the results for three origins of acetone. The average ^{13}C content is very different for each sample, leading to dissimilar intramolecular profiles. However, the slope for each sample is the same, as illustrated in **Figure 15**. Since propylene is the raw material for the two industrial processes used by the main manufacturers (cumene process in the USA and Belgium and direct oxidation of propylene in Japan), it can be concluded that the ^{13}C profile is due to the different propylene source.

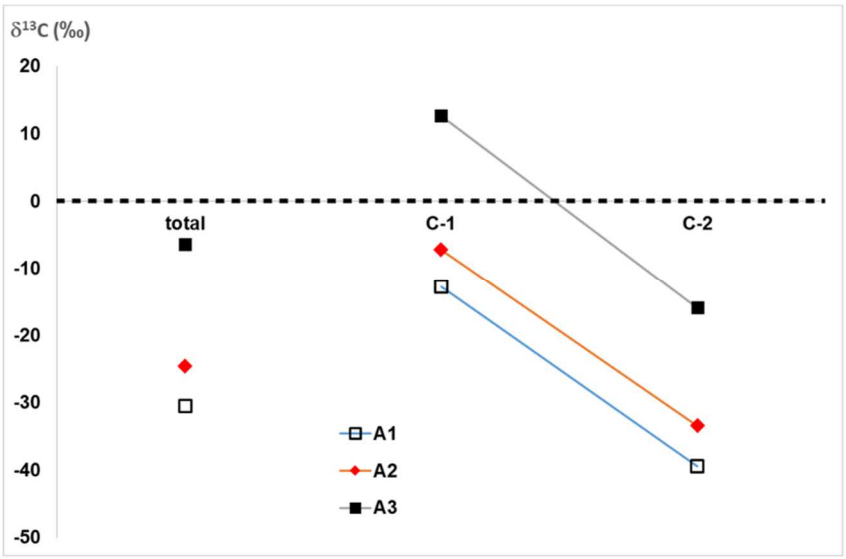

Figure 15: Isotopic composition $\delta^{13}C$ (‰) of the acetone samples (see Table 3 for origins) showing similar slopes for the intramolecular ^{13}C distribution between the samples. Total: global $\delta^{13}C$ value measured by irm-MS. C1: carbonyl position (C=O), C2: methyl position (CH_3). (Adapted from [87]).

5.3.2. Explosives

Among all types of explosive, one category corresponds to pure compounds, including primary explosives (initiators such as organic peroxides) and high explosives like nitro compounds such as trinitrotoluene (TNT). The analytical strategy for explosives usually combines several technologies in order to identify the organic and inorganic substances present both in the explosive and in the post-explosion residues. Isotope analyses are not very common on such compounds, and even less so those using the PSIA strategy. A recent paper employed the latest advanced methodology of irm-NMR to construct ^{13}C and ^{15}N intramolecular profiles of TNT [88]. For irm-^{13}C NMR, the single-pulse method was applied, and for irm-^{15}N NMR, FS-INEPT was utilized [19]. For the latter, FS-INEPT was the only possible choice since ^{15}N has very poor sensitivity (see **Table 2**) and there is no one-bond coupling for polarization transfer in TNT. It was thus the first application of NMR spectroscopy to ^{15}N PSIA (see **Figure 16** for molecular structure and ^{15}N FS-INEPT spectrum).

As a proof of concept, 10 TNT samples collected by the French authorities were studied to compose $\delta^{13}C_i$ (from single-pulse measurement) and apparent $\delta^{15}N_i$ (from FS-INEPT) profiles. It is worth noting here the variation scale of these isotopic compositions.

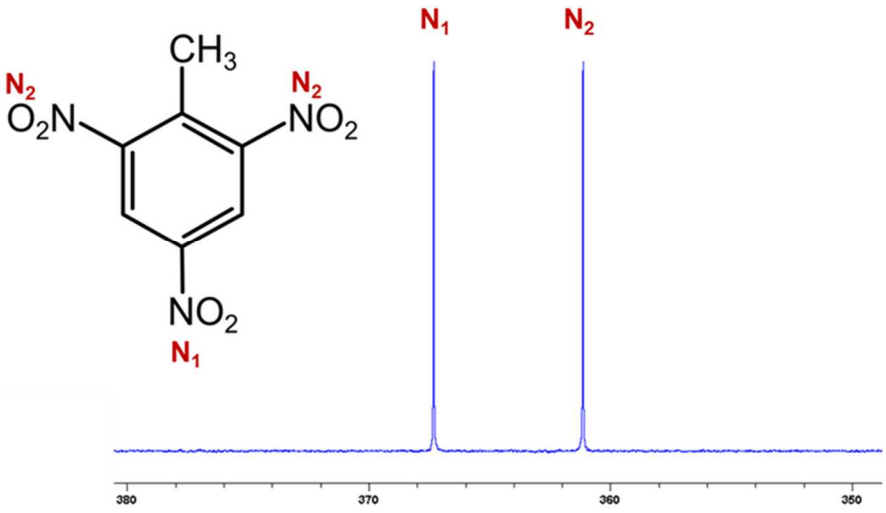

Figure 16: Representation of the TNT molecule with nitrogen positions numbered in decreasing ^{15}N chemical shifts. Typical ^{15}N NMR spectrum of a trinitrotoluene (TNT) sample obtained in about 14 h by adiabatic refocused FS-INEPT ^{15}N with a signal to noise ratio of 500. (Adapted from [88]).

The use of FS-INEPT ^{15}N gives only relative intensities (apparent), but the change in the $\delta^{15}N_i$ value between samples for the same position is still on the correct scale: the difference between two given samples is due solely to the amount of ^{15}N at the given position (the same isotopomer should be compared in the two samples). The change in $\delta^{15}N_i$ can be compared to $\delta^{15}N_g$ to evaluate their respective contribution to the discrimination of origin. For TNT, it was clear that the intramolecular isotopic compositions led to a larger number of discriminating parameters - five for ^{13}C and two for ^{15}N - than the two collected by irm-MS.

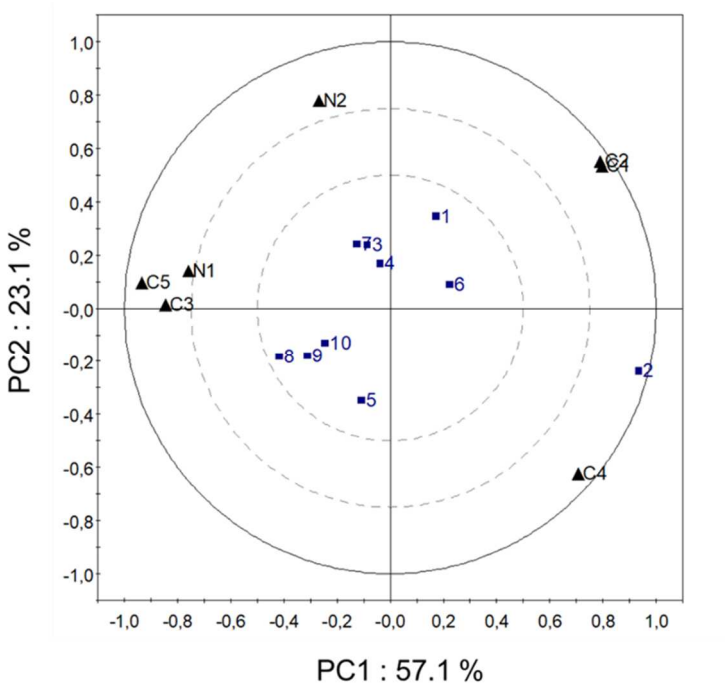

966

967 **Figure 17**: Principal component analysis on TNT samples: PC1 (57.1%) *vs*. PC2 (23.1%) bi-plot (scores + loadings)
968 using the whole experimental variable set from irm-^{15}N NMR (FS-INEPT) and irm-^{13}C NMR (single-pulse)
969 experiments. Triangles represent the loadings (contribution of each measured parameter) used and squares
970 represent the scores (sample identification). The loadings C1 and C2 have the same position. Reprinted with
971 permission from Ref. [88]. Copyright 2020 Elsevier.

972

973 Consequently, resemblances or differences between samples are easily observed in the PCA graph
974 displaying the 10 TNT samples (**Fig. 17**). It should be noted that all the intramolecular parameters (^{13}C
975 and ^{15}N) contribute to the distinction between samples, since they are close to the correlated circle
976 [88].

977 **5.3.3. Drugs**

978 In the field of illicit drugs, forensic investigations have two main objectives: (i) assigning the
979 geographical origin of natural drugs, such as cocaine, heroin and cannabis, and (ii) determining the
980 synthetic route exploited, so as to make the link between precursors and synthetic drugs such as
981 MDMA (ecstasy) and methamphetamine. Most illicit drug samples are imported more or less pure

into Europe and are then gradually diluted along the trafficking chain by the addition of cutting agents. For police investigators, knowing the active principle content is therefore an indication of the proximity of the seized sample to its importation source. The idea of profiling a drug by focusing on the cutting agents, rather than compounds coming from the plant or the manufacturing process, has emerged as a completely new approach. However, regarding pharmaceuticals used as cutting agents, very little has been done with irm-MS, except for acetaminophen and caffeine as cutting agents for heroin.

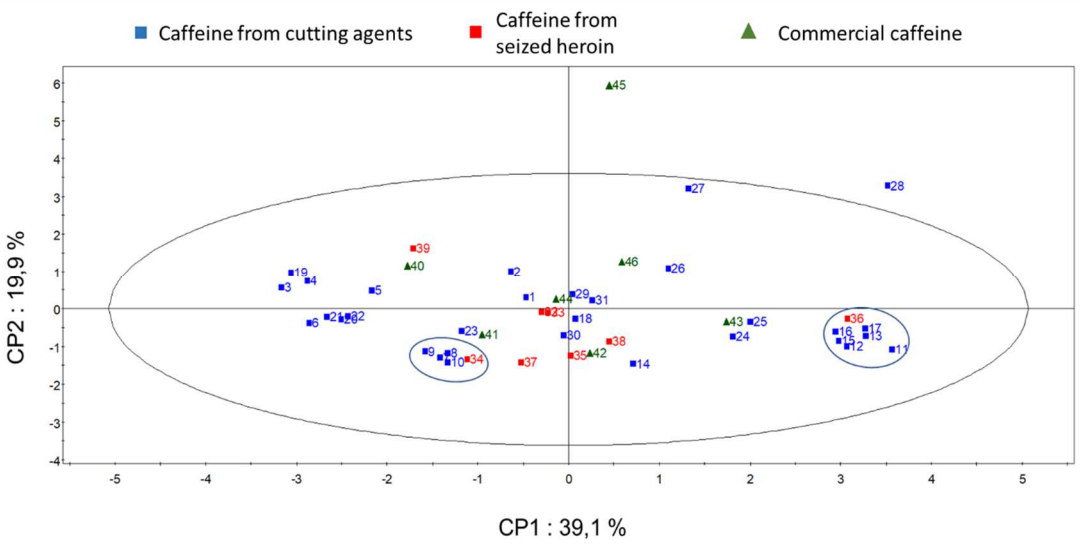

Figure 18: Principal component analysis on caffeine samples from commercial sources, extracted from seized cutting agents and from seized heroin: PC1 (39.1%) *vs*. PC2 (19.9%) score plots using the whole experimental variable set from irm-^{13}C NMR (FS-INEPT) experiments. The interest is to compare the caffeine from cutting agents and from heroin samples. The two encircled zones show the similarity between seized samples: left circle: sample 34 (from heroin) close to samples 7, 8, 9, 10 (from cutting agents from the same seizure); right circle: sample 36 (from heroin) close to samples 11, 12, 13, 15, 16, 17 (from cutting agents from the same seizure). (Adapted from [89]).

The application of irm-^{13}C NMR has provided new information, as shown in a recent work [89]. A prerequisite of the study was to analyze actual seized samples, including both cutting agents and cut heroin. Due to the limited amount available, a specific experimental protocol was established to purify and analyze acetaminophen and/or caffeine samples of only about 40 mg. To study such a small mass, a combination of high magnetic field NMR spectroscopy and FS-INEPT was exploited in order to observe all ^{13}C isotopomers [18, 89]. In fact, the ratio of quaternary to other carbons in these two molecules is not negligible. Moreover, previous analyses (from single-pulse experiments) had shown that these quaternary carbons - three for acetaminophen and four for caffeine - contribute significantly to the discrimination of origin, as described in Sections 5.2 and 5.4.1, respectively [77, 83]. Once again, the isotopic compositions obtained are apparent but suitable for statistical discrimination.

Comparing the isotopic profiles of cutting agents, found pure and the same molecule that was added in the heroin, belonging to the same seizure gives new indications about the affiliation between the trafficking network of heroin and cutting agents. **Figure 18** confirms that the eight ^{13}C isotopomers in caffeine are similarly distributed in samples of pure cutting agents and in cut heroin samples. This is undoubtedly new evidence that will help law authorities to dismantle criminal drug-dealing networks in a country, independently of the origin of the drugs.

5.4. Authentication

In the food industry, authenticity is of particular importance. As a result, a large panel of analytical techniques has been established to protect the health of consumers, guarantee the origin and traceability of products, and fight against fraud, especially against the presence on the market of EMA (Economically Motivated Adulteration). For the consumer, a falsification is a nonconformity of a product with respect to the description on its label. The confirmation of the origin of a product is often performed by isotope analyses because isotopic profiles are usually unique for the “molecule – origin” couple [86]. Three examples are described in this review, to cover three aspects of

authentication issues. The first is the contribution of isotopic NMR to the characterization of the origin of caffeine. The second describes the competition between the increasing complexity of adulteration and the response from the analytical arsenal, illustrated by vanilla flavor and its main molecule, vanillin. The third example concerns the authentication of cholesterol for origin investigation in food products.

5.4.1 Caffeine

Caffeine is found in relatively large amounts in coffee (0.5− 3%), tea (1−4%), mate (0.5−2%), guarana (2−5%), cola species (1−4%), and cocoa (0.1−0.4%), while theobromine is characteristic of cocoa and related *Theobroma* species. Caffeine is also found in energy drinks and cola-type soft drinks, that usually contain added synthetic caffeine. The consumer expects caffeine-containing drinks to be authentic in relation to their declared origin. For cocoa, the geographical origin concerns both the consumers and the chocolate industry.

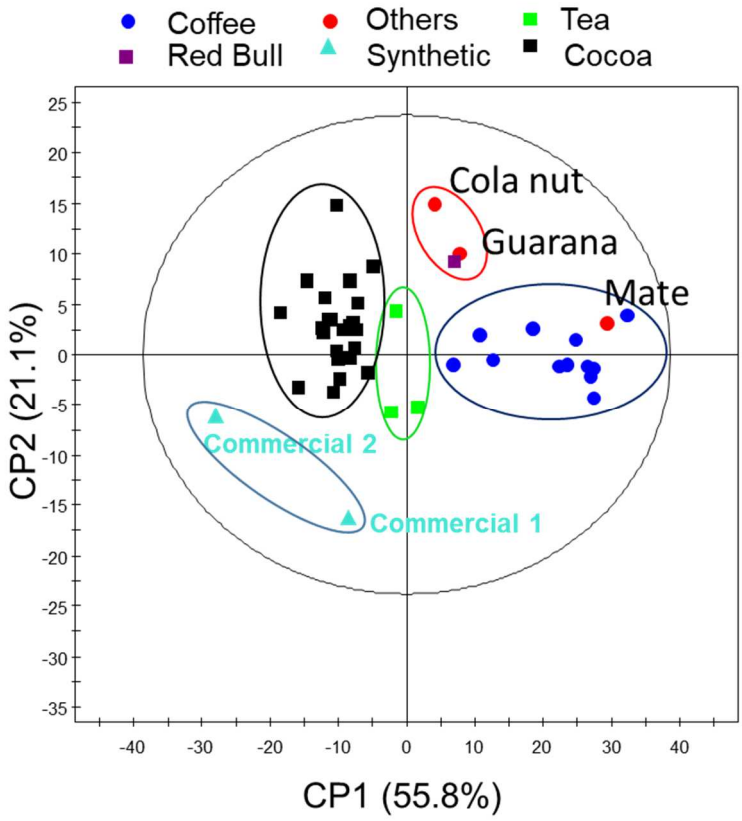

Figure 19: Principal component analysis on caffeine samples from several sources, including theobromine from cocoa: PC1 (55.8%) *vs*. PC2 (21.1%) score plots using the whole experimental variable set from irm-^{13}C NMR (single-pulse) experiments. (Adapted from [77]).

For these two commodities, isotopic compositions contribute fully to the requirements. Within the available methods, irm-^{13}C NMR provides new advances in the discrimination potential. Theobromine, due to its very low solubility in organic solvents typically used for NMR, is not an appropriate molecular probe. A smart approach was developed by the conversion of theobromine to caffeine by methylation [77]. As a result, caffeine is a suitable probe for studying both caffeine-containing matrices and cocoa-based products. It appears that ^{13}C profiles in caffeine are characteristic of both the origins of caffeine-containing products (different plant origins and synthetic caffeine) and of cocoa (geographical origins), as illustrated by **Figure 19.** It should be noted that the application of FS-INEPT to caffeine as described in Section 5.3 led to the same patterns.

5.4.2. Vanillin

A flavor can be defined as a preparation or a substance. Vanilla bean extract is defined as a flavor preparation because it is composed of up to 200 volatile molecules of diverse chemical classes. Vanillin is the main component (about 2% in the plant) and considered a flavor substance. Because of its organoleptic features, vanillin is one of the flavors most used in the food and cosmetics industries, where more than 90% of vanillin is from synthetic origins [90].

An authenticity issue occurs when natural origins are claimed. In the early 1970s, the natural origin was associated with vanilla bean extracts that could be adulterated by vanillin manufactured from guaiacol (ex-guaiacol, synthetic) or from lignin (ex-lignin, semi-synthetic), both with an unnatural status. At that time, the question was: is the vanillin extracted from beans? Irm-^{13}C MS was the answer because the metabolism of vanilla is an example of CAM (Crassulacean Acid Metabolism; see

Section 2.2) leading to $\delta^{13}C_g$ of -20‰ for vanillin while it is in the range from -29‰ to -31‰ for unnatural origins. This is still an official method but it suffers from the easy manipulation of $\delta^{13}C_g$ by the addition of commercially available ^{13}C-enriched vanillin [91]. An effective analytical response was provided by irm-^2H NMR (SNIF-NMR™ methodology) because the four resolved ^2H isotopomers (the OH position cannot be used because of its exchangeable character) were able to distinguish the above three origins: statistically, the detection limit of adulteration was 10-15% (**Fig. 20**) [92]. This method is recognized by official authorities [93].

The last 20 years have witnessed the development of the biosynthesis of natural vanillin from several natural precursors, as depicted in **Figure 21** [94]. The question now is: is the vanillin natural?

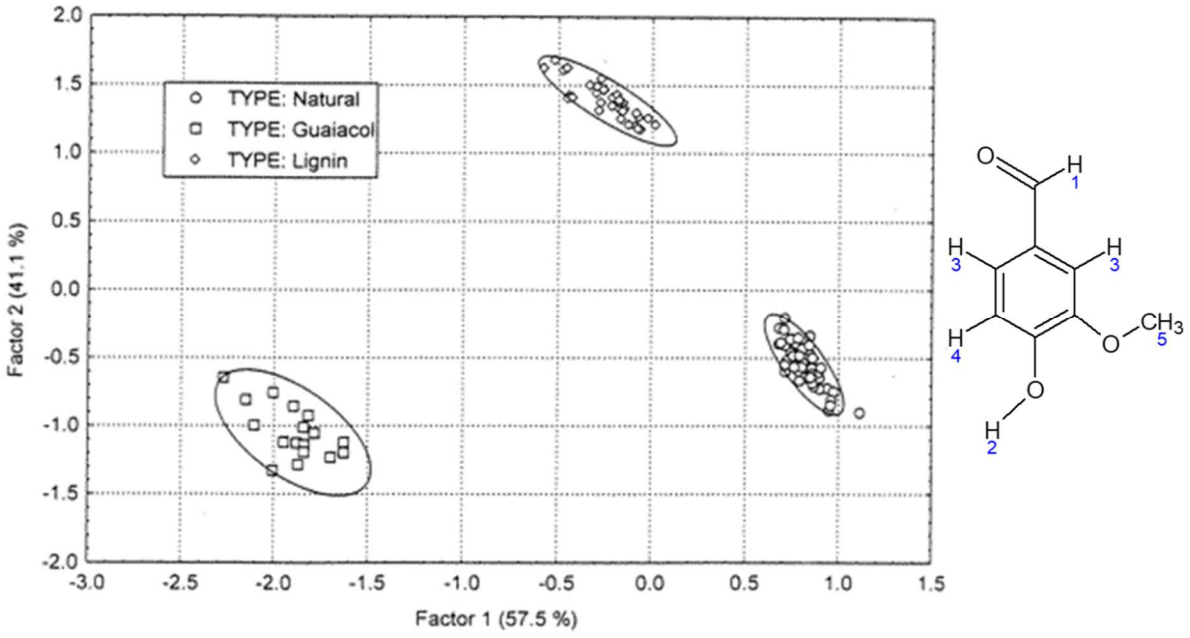

Figure 20: Representation of the reference groups of vanillin (ex-beans, ex-lignin, and ex-guaiacol) projected in the plane of the canonical variables. $(D/H)_1$, $(D/H)_3$, $(D/H)_4$, and $(D/H)_5$ were the initial parameters. The ellipses drawn correspond to the 95% confidence intervals. Representation of the vanillin molecule with the ^2H position numbered in decreasing ^2H chemical shifts. Reprinted with permission from Ref. [92]. Copyright 1997 ACS.

The answer should encompass the isotope profiles of all vanillin sources. In this context, it has been shown that irm-^{2}H NMR is significantly less effective that irm-^{13}C NMR. In fact, the eight ^{13}C isotopomers of vanillin (**Fig. 22**) enable good discrimination between different origins, including the geographical origin of vanilla beans [15]. Another great advantage of ^{13}C NMR over ^{2}H NMR is the smaller quantity of pure vanillin required: 250 mg *versus* 1000 mg, respectively.

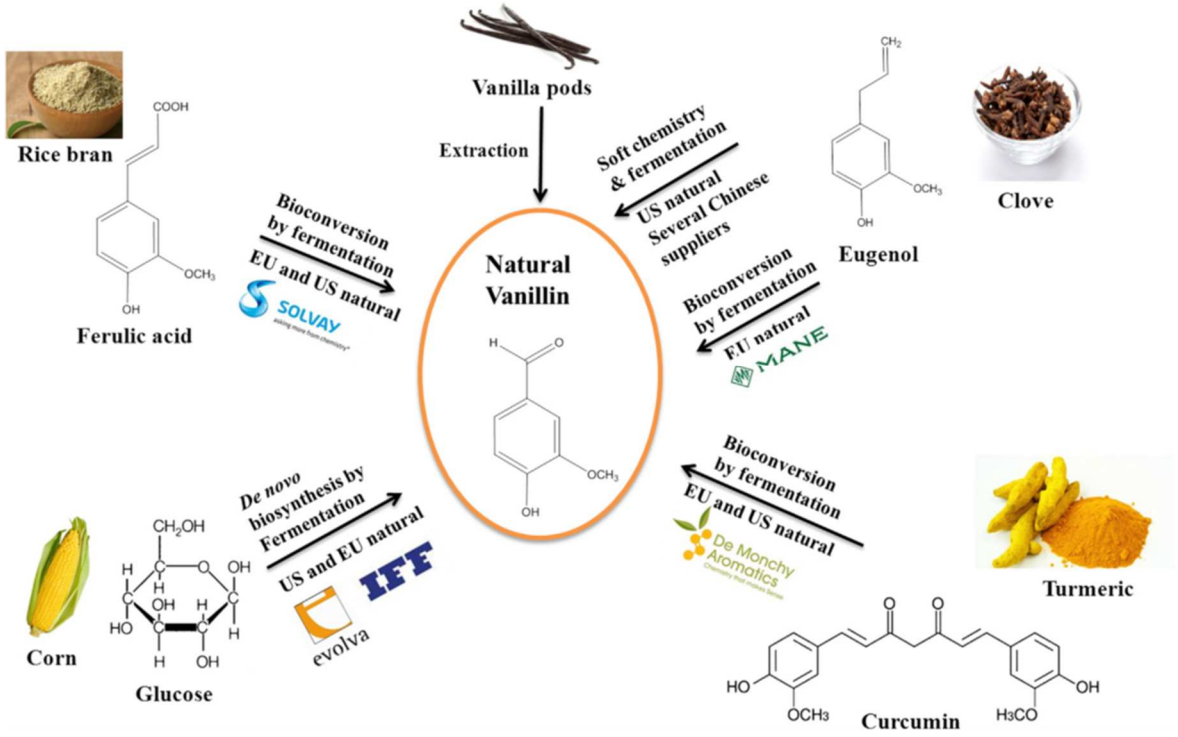

Figure 21: Main sources of vanillin that could be declared as natural. Reprinted with permission from Ref. [94]. Copyright 2015 Elsevier.

In [15], the authors also discuss the positions that led to the best separation of groups, the issue being the contribution of the quaternary carbons. In fact, the five remaining protonated isotopomers were responsible for the main discrimination and thus the INEPT sequence can be easily implemented to decrease the amount of vanillin required for a good precision (as described for other molecules and discussed above). It is therefore possible to study finished products, such as ice

cream, yogurts or vanilla sugars, extending the level of fraud detection from industrial materials only (extracts, flavors) to commercial end-products.

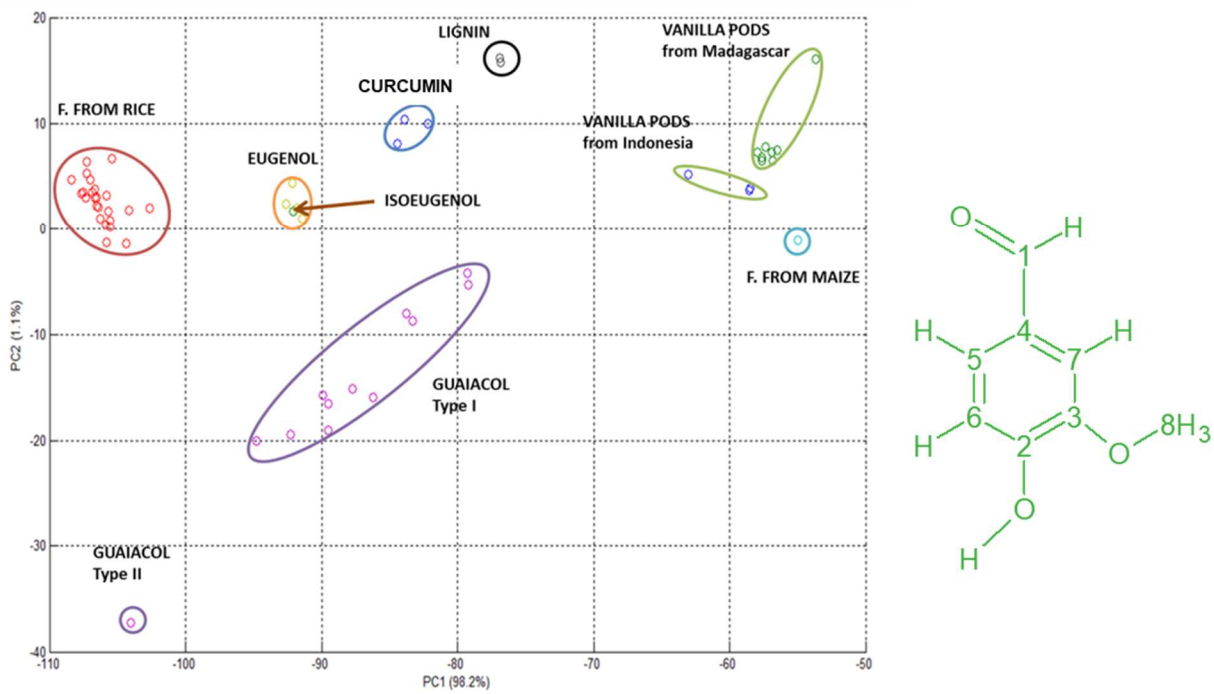

Figure 22: Two-dimensional plot of the scores obtained by PCA on the values of the ^{13}C isotopic composition for all eight isotopomers obtained by irm-^{13}C NMR. PC1 explains 98.2% and PC2 explains 1.1% of the total variability over the main current sources of vanillin. Representation of the vanillin molecule with ^{13}C position numbered in decreasing ^{13}C chemical shifts. Adapted from [15].

5.4.3 Cholesterol

Lipids are known to be quasi-universal components of food products. Their isotopic composition is closely related to geographical origin, botanical origin and agricultural practices in the case of products of plant origin. Cholesterol is one of the most important lipids. It is essential in cellular organization and stability and as a building block for steroid hormones, vitamin D, oxysterols and bile acids. However, cholesterol is also related to many health problems such as cardiovascular disease, diabetes and high blood pressure. Furthermore, it constitutes a good model for the study of steroids.

It has 27 carbon isotopomers, 22 of which are detected by carbon INEPT using one-bond couplings. Positional carbon isotope contents were measured in order to classify egg samples according to their origin [95]. In this work, 90 mg of cholesterol was analyzed using an optimized refocused adiabatic INEPT. As an example of the results described in this article, **Figure 23** shows the classification of eggs from four farming systems with eight variables: one is the global carbon content measured by irm-MS and the others are position-specific ^{13}C contents measured by NMR.

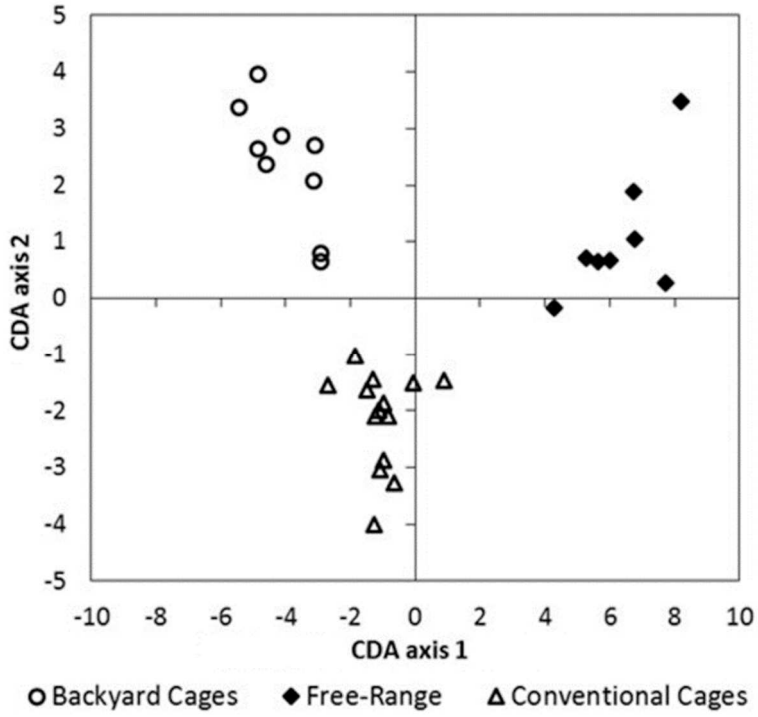

Figure 23: Classification of egg samples according to hen farming system using eight isotopic variables obtained from ^{13}C NMR cholesterol spectra. Adapted from [95].

These results are especially promising since the presented approach can be applied to cholesterol found in other matrices like human blood. In this case, this molecule could be used as a probe to distinguish between exogenous and endogenous sources of cholesterol. This approach could also be applied to other steroids so the field of application can be extended to cover plant and hormone analyses.

5.5. Multi-omics approach

The examples previously described concern pure molecules, but isotopic analysis can also be performed on mixtures and, in these cases, a novel approach called metabisotopomics, merging isotopic and metabolomic profiles, can efficiently be used [57]. It was first applied to the study of triglycerides, which are quasi-universal components of food matrices and consist of complex mixtures [96].

In the carbon spectrum of such a mixture, the peak areas depend on the isotope abundances as well as concentrations. So, to determine the isotope content, it is essential to know the concentration with high precision. In triglycerides, the composition in fatty acids cannot be known with a precision as high as a few permil. Therefore, most of the peaks observed in the ^{13}C NMR spectrum can only be used as compositional profile elements, and not for measurement of the intramolecular isotopic distribution. However, the NMR signals related to the carbons of the glycerol moiety, the first part of the fatty acids (C2 and C3), and the terminal methyl groups, are always present, and are common to all triglyceride molecules. This enables them to be used for isotopic purposes. Isotopic variables can also be obtained from the ratios between two peaks of the same compound. When the SNR is high enough, these two profiles, isotopic and metabolomic, can be obtained from the same carbon spectrum.

This method was applied to classify olive oils according to their geographical origin [96]. Only two ratios are needed, one from the isotopic profile and one from the metabolic profile. The former is the relative isotope abundance of the glycerol carbons and the latter is the relative amount of linoleic acid at the *sn1* or *sn3* position, with respect to that at the *sn2* position. Moreover, full deconvolution of the INEPT spectrum of olive oil provides up to 80 variables (isotopic or metabolomic) which can be used to obtain the complete profile of triglyceride mixtures, *i.e.* oil composition, positional distribution of fatty acids on the glycerol backbone, and some position-

specific ^{13}C content [96]. The same approach can be used to authenticate triacylglycerols of animal origin [95].

This strategy can be extended to 2D NMR, which is an attractive alternative to 1D in order to avoid or limit the overlap of peaks observed in complex mixtures. In order to decrease the experimental time of a 2D acquisition (^{1}H-^{13}C HSQC) a strategy was developed by Merchak *et al.* [50] which consists of choosing, along the indirect dimension, a spectral width smaller than the ^{13}C chemical shift dispersion.

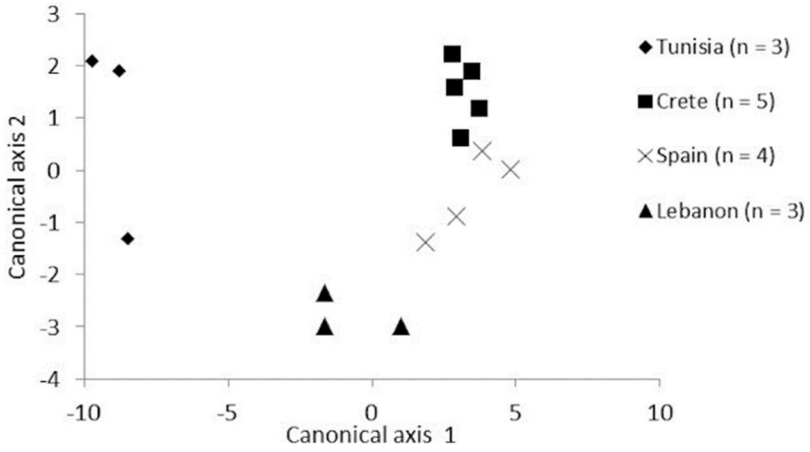

Fig. 24: Classification of vegetable oils using variables from their corresponding HSQC spectra according to their geographical origin. Adapted from [50].

The peaks violating the Nyquist condition are then aliased and the spectral range to be sampled in F_1 is therefore smaller, reducing the number of t_1 increments required to achieve a given F_1 resolution. Additionally, non-uniform sampling is used to halve the number of increments in the F_1 dimension for the same experiment duration, even if it could degrade the reliability of quantitation. With this strategy, the experimental time was reduced to 22 minutes.

Figure 24 shows that such a strategy enables edible oils to be classified according to their geographical or botanical origin [50].

1168

6. Concluding remarks and perspectives

For organic matter, the abundance of ^{2}H, ^{13}C, ^{15}N, ^{18}O or ^{34}S isotopologues -relative to the corresponding lighter species- are routinely determined by irm-MS with a high level of automation. This on-line technique leads to high precision: standard deviation lower than 0.3‰ (on the isotopic composition δ-scale) on a small amount of material (of the order of mg). However, the intramolecular isotopic distribution is not available since only the mean heavy isotope content (global composition) is accessible. However, since a given molecule is constituted of a mixture of isomers (isotopomers), it needs to be taken into account that these could behave independently and differently. Position-specific isotope analysis (PSIA) reveals the isotopomer distribution within a molecule, and NMR spectroscopy is a well-adapted tool for separating the respective signals and quantifying them. Historically, ^{2}H NMR was the first approach able to show the interest of PSIA. Further developments have led to the use of irm-^{13}C NMR and, more recently, irm-^{15}N NMR. Beside the NMR core of this review, in which all parameters are described to establish the optimum protocol, examples of applications of irm-NMR illustrate the information retrieved from typical actual cases and how the analytical protocol should be adapted according to the questions to be addressed.

While a huge amount of information has already been collected, further improvements are on-going. The high precision required imposes significant constraints on NMR experiments. Multi-pulse sequences can be used to overcome these drawbacks and thereby reduce the minimum amount of material needed for irm-^{13}C NMR, or to explore other nuclei, as has been done with ^{15}N.

It is now expected that new challenges will be tackled during the next decade, since preliminary work is converging toward encouraging prospects. Recent advances in 2D NMR promise further improvements in sensitivity, which will allow ^{13}C measurement with only a few mg, or the use of benchtop NMR spectrometers. As an illustration, **Figure 25** shows the 2D spectrum of vanillin obtained on a low-field spectrometer, indicating that in some conditions good precision could be reached for irm-^{13}C NMR on affordable NMR spectrometers for most industrial fields.

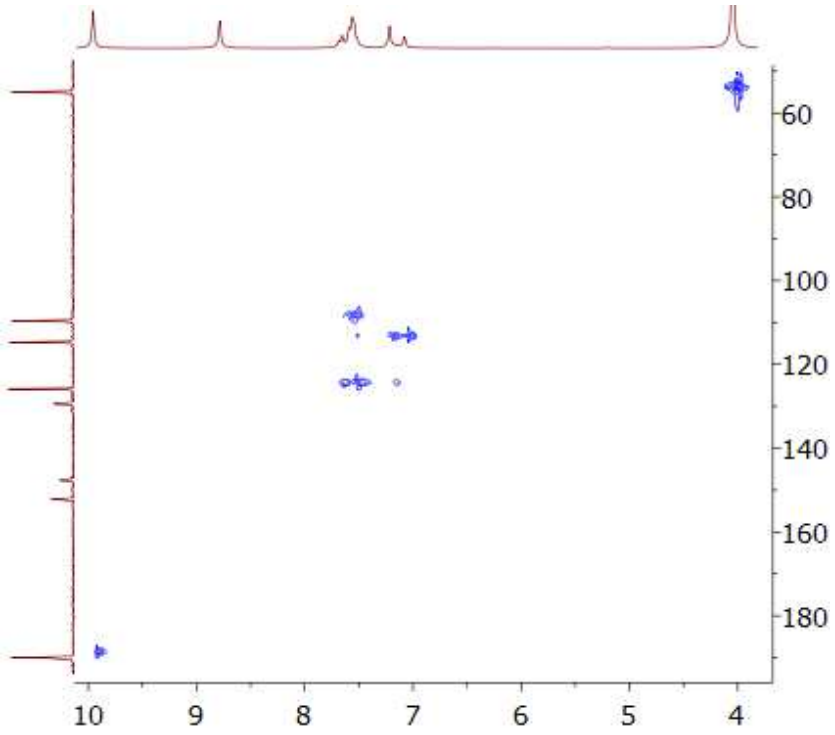

Figure 25: HSQC ^{1}H-^{13}C spectrum of vanillin (215 mg in 0.75 mL of acetone-d_6) obtained on a low-field (80 MHz) Spinsolve spectrometer. Reprinted with permission from Magritek.

PSIA ^{17}O is not yet described in the literature. In the context of the MIF (Mass Independent Fractionation) theory, it could be rewarding to compare the ^{18}O *versus* ^{17}O fractionation in organic matter as it occurs in gases such as O_3, CO_2, N_2O, *etc.* [97]. Beside the interest in ^{17}O, the bi-labeled clumped isotopologue ^{13}C-^{13}C at natural abundance could provide novel information [2].

After reading this review, we hope that new users will join the isotopomics community and contribute to extending such applications, which have already given notable results.

Acknowledgements

The authors thank Carol Wrigglesworth and Richard Robins for fruitful suggestions and linguistic correction. This review was supported by the National Aeronautics and Space Administration through the NASA Astrobiology Institute under Cooperative Agreement No. 80NSSC18M0094 issued through the Science Mission Directorate.

References

1- H.-L. Schmidt, R. J. Robins, R. A. Werner. Multi-factorial in vivo stable isotope fractionation: causes, correlations, consequences and applications. Isotopes Environ. Health Stud. 51 (2015) 155–199. http://dx.doi.org/10.1080/10256016.2015.1014355

2- J. M. Eiler. The Isotopic Anatomies of Molecules and Minerals. Annu. Rev. Earth Planet. Sci. 41 (2013) 411-441. https://doi.org/10.1146/annurev-earth-042711-105348

3- Z. Muccio, G. P. Jackson. Isotope ratio mass spectrometry, Analyst. 134 (2009) 213–222. https://doi:10.1039/B808232D.

4- I. Tea, G. Tcherkez. Natural Isotope Abundance in Metabolites: Techniques and kinetic isotope effect measurement in plant, animal, and human tissues. In: Harris M. E. and Anderson V. E., Editors. Methods in Enzymology (Vol. 596). Cambridge. Academic Press. 2017, pp. 113-147. https:// dx.doi.org/10.1016/bs.mie.2017.07.020

5- R. Dias, K. Freeman, S. Franks. Gas chromatography–pyrolysis–isotope ratio mass spectrometry: a new method for investigating intramolecular isotopic variation in low molecular weight organic acids. Org. Geochem. 33 (2002) 161-168. https://doi.org/10.1016/S0146-6380(01)00141-3

6- C. Gauchotte-Lindsay, S. Turnbull. On-line high-precision carbon position-specific stable isotope analysis: A review. TrAC Trends in Anal. Chem. 76 (2016) 115-125. https://doi.org/10.1016/ j.trac.2015.07.010

7- G. J. Martin, M. L. Martin. Deuterium labelling at the natural abundance level as studied by high field quantitative ^{2}H NMR. Tetrahedron Lett. 22 (1981) 3525-3528. https://doi.org/10.1016/S0040-4039(01)81948-1

8- E. Jamin, F. Thomas. SNIF-NMR Applications in an Economic Context: Fraud Detection in Food Products, in: Mod. Magn. Reson., Springer, Cham, 2017: pp. 1–12. https://doi:10.1007/978-3-319-28275-6_103-1

9- P. Lesot, C. Aroulanda, P. Berdagué, A. Meddour, D. Merlet, J. Farjon, N. Giraud, O. Lafon. Multinuclear NMR in polypeptide liquid crystals: Three fertile decades of methodological developments and analytical challenges. Prog. Nucl. Magn. Reson. Spectrosc. 116 (2020) 85-154. https://doi.org/10.1016/j.pnmrs.2019.10.001

10- J. M. Hayes. Fractionation of the isotopes of carbon and hydrogen in biosynthetic processes. Rev. Mineral Geochem. 43 (2001) 225–277. https://doi.org/10.2138/gsrmg.43.1.225

11- V. Caer, M. Trierweiler, G. J. Martin, M. L. Martin. Determination of site-specific carbon isotope ratios at natural abundance by carbon-13 nuclear magnetic resonance spectroscopy. Anal. Chem. 63 (1991) 2306-2313. https://doi.org/10.1021/ac00020a021

12- B.-L. Zhang, S. Buddrus, M. Trierweiler, G. J. Martin. Characterization of Glycerol from Different Origins by ^{2}H- and ^{13}C-NMR Studies of Site-Specific Natural Isotope Fractionation. J. Agric. Food Chem. 46 (1998) 1374−1380. https://doi.org/10.1021/jf970794+

13- E. Caytan, G. Remaud, E. Tenailleau, S. Akoka. Precise and accurate quantitative ^{13}C NMR with reduced experimental time. Talanta 71 (2007) 1016–1021. https://doi.org/10.1016/j.talanta. 2006.05.075

14- E. Caytan, E. P. Botosoa, V. Silvestre, R. J. Robins, S. Akoka, G. S. Remaud. Accurate Quantitative ^{13}C NMR Spectroscopy: Repeatability over Time of Site-Specific ^{13}C Isotope Ratio Determination. Anal. Chem. 79 (2007) 8266-8269. https://doi.org/10.1021/ac070826k.

15- S. Guyader, F. Thomas, E. Jamin, M. Grand, S. Akoka, V. Silvestre, G. S. Remaud. Combination of ^{13}C and ^{2}H SNIF-NMR isotopic fingerprints of vanillin to control its precursors. Flavour Fragr. J. 34 (2019) 133-144. https://doi: 10.1002/ffj.3486

16- C. Thibaudeau, G. S. Remaud, V. Silvestre, S. Akoka. Performance Evaluation of Quantitative Adiabatic ^{13}C NMR Pulse Sequences for Site-Specific Isotopic Measurements. Anal. Chem. 82 (2010) 5582-5590. https://doi.org/10.1021/ac100478h.

17- G. Tcherkez, J. Ghashghaie, H. Griffiths. Methods for improving the visualization and deconvolution of isotopic signals. Plant Cell Environ. 30 (2007) 887–891. https://dx.doi: 10.1111/j.1365-3040.2007.01687.x

18- V. Joubert, V. Silvestre, M. Grand, D. Loquet, V. Ladroue, F. Besacier, S. Akoka, G. S. Remaud. Full spectrum isotopic ^{13}C NMR using polarization transfer for position-specific isotope analysis. Anal. Chem. 90 (2018) 8692–8699. https://pubs.acs.org/doi/10.1021/acs.analchem.8b02139.

19- V. Joubert, V. Silvestre, M. Lelièvre, V. Ladroue, F. Besacier, S. Akoka, G. S. Remaud. Position-specific ^{15}N isotope analysis in organic molecules: A high-precision ^{15}N NMR method to determine the intramolecular ^{15}N isotope composition and fractionation at natural abundance. Magn. Reson. Chem. 57 (2019) 1136–1142. DOI: 10.1002/mrc.4903

20- T. B. Coplen, Guidelines and recommended terms for expression of stable-isotope-ratio and gas-ratio measurement results. Rapid Commun. Mass Spectrom. 25 (2011) 2538–2560. https://doi.org/ 10.1002/rcm.5129

21- T. Jézéquel, V. Joubert, P. Giraudeau, G. S. Remaud, S. Akoka. The new face of isotopic NMR at natural abundance. Magn. Reson. Chem. 55 (2017) 77-90. https://doi.org/10.1002/mrc.4548

22- G. S. Remaud, S. Akoka. Review of flavors authentication by position-specific isotope analysis by nuclear magnetic resonance spectrometry: the example of vanillin. Flavour Frag. J. 32 (2017) 77-84. https://doi.org/10.1002/ffj.3366

23- I. D. Clark (1998) Isotope fractionation. In: Geochemistry. Encyclopedia of Earth Science. Springer, Dordrecht. https://doi.org/10.1007/1-4020-4496-8

24- G. D. Farquhar, J. R. Ehleringer, K. T. Hubick. Carbon Isotope Discrimination and Photosynthesis. Annu. Rev. Plant Physiol. Plant Mol. Biol. 40 (1989) 503-537. https://doi.org/10.1146/annurev.pp.40. 060189.002443

25- T. B. Hofstetter, M. Berg. Assessing transformation processes of organic contaminants by compound-specific stable isotope analysis. Trends Anal. Chem. 30 (2011) 618–627. https:// doi.org/10.1016/j.trac.2010.10.012.

26- M. Thullner, F. Centler, H.-H. Richnow, A. Fischer. Quantification of organic pollutant degradation in contaminated aquifers using compound specific stable isotope analysis – Review of recent developments. Org. Geochem. 42 (2012) 1440–1460. https://doi.org/ 10.1016/j.orggeochem. 2011.10.011

27- D. Bouchard, D. Hunkeler, P. Höhener. Carbon isotope fractionation during aerobic biodegradation of n-alkanes and aromatic compounds in unsaturated sand. Org. Geochem. 39 (2008) 23-33. https:// doi.org/10.1016/j.orggeochem.2007.10.002.

28- P. H. Abelson, T. C. Hoering. Carbon isotope fractionation in formation of amino acids by photosynthetic organisms. Proc. Natl. Acad. Sci. U.S.A. 47 (1961) 623-632. https://doi.org/10.1073/pnas.47.5.623.

29- K. Yamada, M. Tanaka, F. Nakagawa, N. Yoshida. On-line measurement of intramolecular carbon isotope distribution of acetic acid by continuous-flow isotope ratio mass spectrometry. Rapid Commun. Mass Spectrom. 16 (2002) 1059–1064. https://doi.org/10.1002/rcm.678.

30- J. M. Eiler, B. Bergquist, I. Bourg, P. Cartigny, J. Farquhar, A. Gagnon, W. Guo, I. Halevy, A. Hofmann, T. E. Larson, N. Levin, E. A. Schauble, D. Stolper. Frontiers of stable isotope geoscience. Chem. Geol. 372 (2014) 119–143. https://doi.org/10.1016/j.chemgeo.2014.02.006.

31- G. S. Remaud, P. Giraudeau, P. Lesot, S. Akoka. Isotope Ratio Monitoring by NMR. Part 1: Recent Advances. In: Webb G. (eds) Modern Magnetic Resonance. Springer, Cham, 2017.

32- A. Menditto, M. Patriarca, B. Magnusson. Understanding the meaning of accuracy, trueness and precision. Accred. Qual. Assur. 12 (2007) 45–47. https://doi.org /10.1007/s00769-006-0191-z

33- JCGM: Joint Committee for Guides in Metrology, International vocabulary of metrology – Basic and general concepts and associated terms (VIM). JCGM 200:2012.

34- E. Prenesti, F. Gosmaro. Trueness, precision and accuracy: a critical overview of the concepts as well as proposals for revision. Accred. Qual. Assur. 20 (2015) 33–40. https://doi.org/10.1007/s00769-014-1093-0

35- P. Giraudeau, I. Tea, G. Remaud, S. Akoka. Reference and normalization methods: Essential tools for the intercomparison of NMR spectra. J. Pharm. Biomed. Anal. 93 (2014) 3–16. http://dx.doi.org/10.1016/j.jpba.2013.07.020

36- R. R. Ernst, G. Bodenhausen, A. Wokaun. Principles of Nuclear Magnetic Resonance in One and Two Dimensions, Oxford University Press, New York, 1991.

37- D. J. Cookson, B. E. Smith. Optimal conditions for obtaining quantitative ^{13}C NMR Data. J. Magn. Reson. 57 (1984) 355-368. https://doi.org/10.1016/0022-2364(84)90253-1.

38- S. Gillet, J.-J. Delpuech. Optimum conditions for nondestructive quantitative analysis by carbon-13 NMR. J. Magn. Reson. 38 (1980) 433-445. https://doi.org/10.1016/0022-2364(80)90325-X

39- D. J. Cookson, B. E. Smith. Optimal experimental parameters for quantitative pulse Fourier transform proton nuclear magnetic resonance spectrometry. Anal. Chem. 54 (1982) 2591–3. https://doi.org/ 10.1021/ac00251a042

40- E. Tenailleau, G. S. Remaud, S. Akoka. Quantification of the ^{1}H-decoupling effects on the accuracy of ^{13}C-NMR measurements. Instrum. Sci. Technol. 33 (2005) 391-399. https://doi.org/10.1081/CI-200063700.

41- E. Tenailleau, S. Akoka. Adiabatic ^{1}H decoupling scheme for very accurate intensity measurements in ^{13}C-NMR. J. Magn. Reson. 185 (2007) 50-58. https://doi.org/10.1016/j.jmr.2006.11.007

42- F. Schilling, L. R. Warner, N. I. Gershenzon, T. E. Skinner, M. Sattler, S. J. Glaser. Next-generation heteronuclear decoupling for high-field biomolecular NMR spectroscopy. Angew. Chem. Int. Ed. 53 (2014) 4475-4479. https://doi.org/10.1002/anie.201400178

43- A. Tannus, M. Garwood. Improved performance of frequency-swept pulses using offset-independent adiabaticity. J. Magn. Reson. A 120 (1996) 133–137. https://doi.org/10.1006/jmra.1996.0110.

44- N. Karabulut, E. Baguet, M. Trierweiler, S. Akoka**.** Improvement in quantitative accuracy of 13C DEPT integrals by parameter-optimization. Anal. Lett. 35 (2002) 2549–2563. https://doi.org/10.1081/AL-120016544

45- T. Saito, S. Nakaie, M. Kinoshita, T. Ihara, S. Kinugasa, A. Nomura, T. Maeda. Practical guide for accurate quantitative solution state NMR analysis. Metrologica 41 (2004) 213-218. https://doi.org/10.1088/0026-1394/41/3/015

46- U. Holzgrabe. Quantitative NMR spectroscopy in pharmaceutical applications. Prog. Nucl. Magn. Reson. Spectrosc. 57 (2010) 229-240. https://doi.org/10.1016/j.pnmrs.2010.05.001.

47- S. K. Bharti, R. Roy. Quantitative ^{1}H NMR spectroscopy. TrAC Trends Anal. Chem. 35 (2012) 5-26. https://doi.org/10.1016/j.trac.2012.02.007.

48- R. J. Robins, G. S. Remaud, S. Akoka. Isotope Ratio Monitoring ^{13}C Nuclear Magnetic Resonance Spectrometry for the Analysis of Position-Specific Isotope Ratios. In: Harris M. E. and Anderson V. E., Editors. Methods in Enzymology (Vol. 596). Cambridge. Academic Press, 2017.

49- U. Bussy, C. Thibaudeau, F. Thomas, J.-R. Desmurs, E. Jamin, G. S. Remaud, V. Silvestre, S. Akoka. Isotopic finger-printing of active pharmaceutical ingredients by ^{13}C NMR and polarization transfer techniques as a tool to fight against counterfeiting. Talanta 85 (2011) 1909-1914. https://doi.org/10.1016/j.talanta.2011.07.022.

50- N. Merchak, V. Silvestre, L. Rouger, P. Giraudeau, T. Rizk, J. Bejjani, S. Akoka. Precise and rapid isotopomic analysis by ^{1}H-^{13}C 2D NMR: Application to triacylglycerol matrices. Talanta 156-157 (2016) 239-244. https://doi.org/10.1016/j.talanta.2016.05.031.

51- A. Chaintreau, W. Fieber, H. Sommer, A. Gilbert, K. Yamada, N. Yoshida, A. Pagelot, D. Moskau, A. Moreno, J. Schleucher, F. Reiniero, M. Holland, C. Guillou, V. Silvestre, S. Akoka, G. S. Remaud. Site-specific ^{13}C content by quantitative isotopic ^{13}C Nuclear Magnetic Resonance Spectrometry: a pilot inter-laboratory study. Anal. Chim. Acta 788 (2013) 108–113. https://doi.org/10.1016/j.aca.2013.06.004.

52- E. Martineau, S. Akoka, R. Boisseau, B. Delanoue, P. Giraudeau. Fast Quantitative ^{1}H–^{13}C Two-Dimensional NMR with Very High Precision. Anal. Chem. 85 (2013) 4777-4783. https://doi.org/10.1021/ac4005309.

53- T. Schoenberger, S. Menges, M.A. Bernstein. Improving the performance of high-precision qNMR measurements by a double integration procedure in practical cases. Anal. Chem. 88 (2016) 3836–3843. https://doi.org/10.1021/acs.analchem.5b04911

54- R. Laatikainen, M. Tiainen, S.-P. Korhonen, M. Niemitz. Computerized Analysis of High-resolution Solution-state Spectra. Encyclopedia of Magnetic Resonance on line, John Wiley & Sons; 2011. https://doi.org/10.1002/9780470034590.emrstm1226.

55- S. Sokolenko, T. Jezequel, G. Hajjar, J. Farjon, S. Akoka, P. Giraudeau. Robust 1D NMR lineshape fitting using real and imaginary data in the frequency domain. J. Magn. Reson. 298 (2019) 91-100. https://doi.org/10.1016/j.jmr.2018.11.004.

56- E. Tenailleau, P. Lancelin, R. J. Robins, S. Akoka, Authentication of the origin of vanillin using quantitative natural abundance ^{13}C NMR. J. Agric. Food Chem. 52 (2004) 7782-7787. https://doi.org/10.1021/jf048847s.

57- N. Merchak, J. Bejjani, T. Rizk, V. Silvestre, G. S. Remaud, S. Akoka. ^{13}C isotopomics of triacylglycerols using NMR with polarization transfer techniques. Anal. Methods 7 (2015) 4889–4891. https://doi.org/10.1039/C5AY01250C.

58- M. L. Martin, S. Akoka, G. J. Martin, SNIF-NMR – Part 1: Principles. In: Webb G. A., editor. Modern magnetic resonance. Dordrecht: Springer; 2006.

59- C. Fauhl, R. Z. Wittkowski. On line H-1-NMR to facilitate tube preparation in SNIF-NMR analysis. Z. Lebensm. Unters. Forsch. 203 (1996) 541–5. https://doi.org/10.1007/BF01193160.

60- T. Jézéquel, V. Silvestre, K. Dinis, P. Giraudeau, S. Akoka. Optimized slice-selective ^{1}H NMR experiments combined with highly accurate quantitative ^{13}C NMR using an internal reference method. J. Magn. Res. 289 (2018) 18-25. https://doi.org/10.1016/j.jmr.2018.02.002

61- K. Bayle, M. Grand, A. Chaintreau, R. J. Robins, W. Fieber, H. Sommer, S. Akoka, G. S. Remaud. Internal referencing for ^{13}C position-specific isotope analysis measured by NMR spectrometry. Anal. Chem. 87 (2015) 7550-4. https://doi.org/10.1021/acs.analchem.5b02094.

62- B.-L. Zhang, M. Trierweiler, C. Jouitteau, G. J. Martin. Consistency of NMR and Mass Spectrometry determinations of natural abundance site-specific carbon isotope ratios. The case of Glycerol. Anal. Chem. 71 (1999) 2301-2306. https://doi.org/10.1021/ac9812375.

63- A. Gilbert, R. Hattori, V. Silvestre, N. Wasano, S. Akoka, S. Hirano, K. Yamada, N. Yoshida, G. S. Remaud. Comparison of IRMS and NMR spectrometry for the determination of intramolecular ^{13}C isotope composition: Application to ethanol. Talanta 99 (2012) 1035–1039. http://dx.doi.org/ 10.1016/ j.talanta.2012.05.023

64- K. Bayle, A. Gilbert, M. Julien, K. Yamada, V. Silvestre, R. J. Robins, S. Akoka, N. Yoshida, G. S. Remaud. Conditions to obtain precise and true measurements of the intramolecular ^{13}C distribution in organic molecules by isotopic ^{13}C nuclear magnetic resonance spectrometry. Anal. Chim. Acta 846 (2014) 1–7. https://doi.org/10.1016/j.aca.2014.07.018

65- B. Fry, J. F. Carter, K. Yamada, N. Yoshida, D. Juchelka. Position-specific ^{13}C/^{12}C analysis of amino acid carboxyl groups – automated flow-injection analysis based on reaction with ninhydrin. Rapid Commun. Mass Spectrom. 32 (2018) 992–1000. https://doi.org/10.1002/rcm.8126

66- A. P. Crawley, R. M. Henkemman. A comparison of one-shot and recovery methods in T1 imaging. Magn. Reson. Med. 7 (1988) 23-34. https://doi.org/10.1002/mrm.1910070104.

67- C. Liu, G. P. McGovern, P. Liua, H. Zhao, J. Horita. Position-specific carbon and hydrogen isotopic compositions of propane from natural gases with quantitative NMR. Chem. Geol. 491 (2018) 14-26. https://doi.org/10.1016/j.chemgeo.2018.05.011

68- T. Wieloch, I. Ehlers, J. Yu, D. Franck, M. Grabner, A. Gessler, J. Schleucher. Intramolecular ^{13}C analysis of tree rings provides multiple plant ecophysiology signals covering decades. Sci. Rep. 8 (2018) 5048 (10 pages). https://doi.org/10.1038/s41598-018-23422-2

69- D. Hoffman, C. Rasmussen. Position-Specific carbon stable isotope ratios by proton NMR spectroscopy. Anal. Chem. 91 (2019) 15661-15669. Doi: 10.1021/acs.analchem. 9b03776

70- E. P. Botosoa, E. Caytan, V. Silvestre, R. J. Robins, S. Akoka, G. S. Remaud. Unexpected Fractionation in Site-Specific ^{13}C Isotopic Distribution Detected by Quantitative ^{13}C NMR at Natural Abundance. J. Am. Chem. Soc. 130 (2008) 414-415. https://doi.org/10.1021/ja0771181

71- M. Julien, J. Parinet, P. Nun, K. Bayle, P. Höhener, R. J. Robins, G. S. Remaud. Fractionation in position-specific isotope composition during vaporization of environmental pollutants measured with isotope ratio monitoring by ^{13}C nuclear magnetic resonance spectrometry. Environ. Pollut. 205 (2015) 299-306. http://dx.doi.org/10.1016/j.envpol.2015.05.047

72- M. Julien, P. Höhener, R. J. Robins, J. Parinet, G. S. Remaud. Position-Specific ^{13}C Fractionation during Liquid−Vapor Transition Correlated to the Strength of Intermolecular Interaction in the Liquid Phase. J. Phys. Chem. B 121 (2017) 5810−5817. DOI: 10.1021/acs.jpcb.7b00971

73- E. P. Botosoa, V. Silvestre, R. J. Robins, J. M. Moreno Rojas, C. Guillou, G. S. Remaud. Evidence of ^{13}C non-covalent isotope effects obtained by quantitative ^{13}C nuclear magnetic resonance spectroscopy at natural abundance during normal phase liquid chromatography. J. Chromatogr. A 1216 (2009) 7043–7048. doi:10.1016/j.chroma.2009.08.066

74- E. Cicchetti, V. Silvestre, W. Fieber, H. Sommer, G. Remaud, S. Akoka, A. Chaintreau. Procedure for the isolation of vanillin from vanilla extracts prior to isotopic authentication by quantitative ^{13}C-NMR. Flavour Fragr. J. 25 (2010) 463–467. DOI 10.1002/ffj.2006

75- E. P. Botosoa, C. Blumenstein, D. A. MacKenzie, V. Silvestre, G. S. Remaud, R. A. Kwiecień, R. J. Robins. Quantitative isotopic ^{13}C nuclear magnetic resonance at natural abundance to probe enzyme reaction mechanisms via site-specific isotope fractionation: The case of the chain-shortening reaction for the bioconversion of ferulic acid to vanillin. Anal. Biochem. 393 (2009) 182–188. doi:10.1016/j.ab.2009.06.031

76- A. Gilbert, R. J. Robins, G. S. Remaud, G. B. Tcherkez. Intramolecular ^{13}C pattern in hexoses from autotrophic and heterotrophic C3 plant tissues. Proc. Natl. Acad. Sci. U. S. A. 109 (2012) 18204–18209. https://doi.org/10.1073/pnas.1211149109

77- D. G. Diomande, E. Martineau, A. Gilbert, P. Nun, A. Murata, K. Yamada, N. Watanabe, I. Tea, R. J. Robins, N. Yoshida, G. S. Remaud. Position-Specific Isotope Analysis of Xanthines: A ^{13}C Nuclear Magnetic Resonance Method to Determine the ^{13}C Intramolecular Composition at Natural Abundance. Anal. Chem. 87 (2015) 6600−6606. DOI: 10.1021/acs.analchem.5b00559

78- WHO 2017, http://www.who.int/medicines/regulation/ssffc/definitions/en/, consulted 1st April 2020

79- K. Dégardin, Y. Roggo, P. Margot. Forensic intelligence for medicine anti-counterfeiting. Forensic Sci. Int. 248 (2015) 15-17. https://doi.org/10.1016/j.forsciint.2014.11.015

80- J. P. Jasper, B. J. Westenberger, J. A. Spencer, L. F. Buhse, M. Nasr. Stable isotopic characterization of active pharmaceutical ingredients. J. Pharm. Biomed. Anal. 35 (2004) 21-29. https://doi.org/10.1016/ S0731-7085(03)00581-8

81- T. Gilveska, M. Gehre, H. H. Richnow. Multidimensional isotope analysis of carbon, hydrogen and oxygen as tool for identification of the origin of ibuprofen. J. Pharm. Biomed. Anal. 115 (2015) 410–416. https://doi.org/10.1016/j.jpba.2015.07.030

82- J. Gooch, B. Daniel, V. Abbate, N. Frascione. Taggant materials in forensic science: A review. TrAC Trends Anal. Chem. 83 (2016) 49-5. https://doi.org/10.1016/j.trac.2016.08.003

83- V. Silvestre, V. Maroga Mboula, C. Jouitteau, S. Akoka, R. J. Robins, G. S. Remaud. Isotopic ^{13}C NMR spectrometry to assess counterfeiting of active pharmaceutical ingredients: Site-specific ^{13}C content of aspirin and paracetamol. J. Pharm. Biomed. Anal. 50 (2009) 336-341. https://doi.org/10.1016/j.jpba.2009.04.030

84- G. S. Remaud, U. Bussy, M. Lees, F. Thomas, J.-R. Desmurs, E. Jamin, V. Silvestre, S. Akoka. NMR spectrometry isotopic fingerprinting: A tool for the manufacturer for tracking Active Pharmaceutical Ingredients from starting materials to final medicines. Eur. J. Pharm. Sci. 48 (2013) 464–473. http://dx.doi.org/10.1016/j.ejps.2012.12.009

85- D. Acetti, E. Brenna, G. Fronza, C. Fuganti. Monitoring the synthetic procedures of commercial drugs by ^{2}H NMR spectroscopy: the case of ibuprofen and naproxen. Talanta 76 (2008) 651–655. https://doi.org/10.1016/j.talanta.2008.04.009

86- N. Gentile, R. T. W. Siegwolf, P. Esseiva, S. Doyle, K. Zollinger, O. Delémont. Isotope ratio mass spectrometry as a tool for source inference in forensic science: A critical review. Forensic Sci. Internat. 251 (2015) 139–158. https://doi.org/10.1016/j.forsciint.2015.03.031

87- M. Julien, P. Nun, P. Höhener, J. Parinet, R. J. Robins, G. S. Remaud. Enhanced forensic discrimination of pollutants by position-specific isotope analysis using isotope ratio monitoring by ^{13}C nuclear magnetic resonance spectrometry. Talanta 147 (2016) 383-389. https://doi.org/10.1016/ j.talanta.2015.10.010

88- V. Joubert, V. Silvestre, V. Ladroue, F. Besacier, P. Blondel, S. Akoka, E. Baguet, G. S. Remaud. Forensic application of position-specific isotopic analysis of trinitrotoluene (TNT) by NMR to determine ^{13}C and ^{15}N intramolecular isotopic profiles. Talanta, 2020, in press. https://doi.org/ 10.1016/j.talanta.2020.120819

89- V. Joubert, M. Trébuchet, M. Mikic, V. Silvestre, A.-M. Schiphorst, D. Loquet, A. Stemmelen, V. Ladroue, F. Besacier, S. Akoka, G. S. Remaud. Isotopomics by isotope ratio monitoring by ^{13}C nuclear magnetic resonance spectrometry on cutting agents in heroin: A new approach for illicit drugs trafficking route elucidation. Drug Test. Anal., 2020, in press. https://doi.org/10.1002/dta.2745

90- M. M. Bomgardner. The problem with vanilla. Chem. Eng. News 94 (2016) 38-42.

91- J. Bricout, J. Koziet, M. Derbesy, B. Becat. Nouvelles possibilités de l'analyse des isotopes stables du carbone dans le contrôle de la qualité des vanilles. Ann. Fals. Exp. Chim. 74 (1981) 691-696.

92- G. S. Remaud, Y.-L. Martin, G. G. Martin, G. J. Martin. Detection of Sophisticated Adulterations of Natural Vanilla Flavors and Extracts: Application of the SNIF-NMR Method to Vanillin and p-Hydroxybenzaldehyde. J. Agric. Food Chem. 45 (1997) 859-866. https://doi.org/10.1021/jf960518f

93- E. Jamin, F. Martin, G. G. Martin, A.-I. Fauhl. Determination of Site-Specific (Deuterium/ Hydrogen) Ratios in Vanillin by ^{2}H-Nuclear Magnetic Resonance Spectrometry: Collaborative Study. J. AOAC Int. 90 (2007) 187-195. https://doi.org/10.1093/jaoac/90.1.187

94- N. J. Gallage, B. L. Møller. Vanillin–bioconversion and bioengineering of the most popular plant flavor and its de novo biosynthesis in the vanilla orchid. Molecular Plant. 8 (2015) 40-57. https://doi.org/10.1016/j.molp.2014.11.008

95- G. Hajjar, T. Rizk, J. Bejjani, S. Akoka. Metabisotopomics of triacylglycerols from animal origin: A simultaneous metabolomic and isotopic profiling using ^{13}C INEPT. Food Chem. 315 (2020) 126325. https://doi.org/10.1016/j.foodchem.2020.126325

96- N. Merchak, T. Rizk, V. Silvestre, G. S. Remaud, J. Bejjani, S. Akoka. Olive oil characterization and classification by ^{13}C-NMR with a polarization transfer technique: A comparison with gas chromatography and ^{1}H-NMR. Food Chem. 245 (2018) 717-723. https://doi.org/10.1016/ j.foodchem.2017.12.005

97- M. H. Thiemens. Introduction to Chemistry and Applications in Nature of Mass Independent Isotope Effects Special Feature. Proc. Natl. Acad. Sci. U. S. A. 110 (2013) 17631-17637. https://doi.org/ 10.1073/pnas.1312926110

1502 # Glossary of abbreviations

Acronyms and symbols for NMR

β	Flip angle
$\vec{B}_0$	Static magnetic field
$\vec{B}_1$	RF magnetic field
$\vec{B}_2$	RF magnetic field during decoupling
γ	Magnetogyric ratio
DEPT	Distortionless enhancement by polarization transfer
DMSO-d_6	Dimethylsulfoxide fully deuterated
FS-INEPT	Full spectrum insensitive nuclei enhancement by polarization transfer
Γ	Difference from 1 in the ratio of CH_2/CH_3 in ^{13}C bi-labeled ethanol
HSQC	Heteronuclear single quantum coherence
i	Position of the atom within the molecule (found also as site)
INEPT	Insensitive nuclei enhancement by polarization transfer
M	Magnetization
M_{eq}	Magnetization at equilibrium (steady state)
nD	NMR at dimension n
n_i	Equivalent number of nuclei at position i
NMR	Nuclear magnetic resonance
nOe	Nuclear Overhauser effect
OIA	Offset-independent-adiabaticity
Ω	Signal offset
qNMR	Quantitative Nuclear magnetic resonance
RF	Radio-frequency
S	Area of NMR peak

SNR	Signal-to-noise ratio
Ta	Analysis time
T_1	Longitudinal relaxation time
T_2	Transverse relaxation time
TI	Inversion time
TR	Repetition time: delay between consecutive acquisition in the pulse sequence
ω_1	Amplitude ($\gamma.B_1$) in Hertz of RF pulses
ω_2	Amplitude (γ.B2) in Hertz of RF pulses during heteronuclear decoupling
WALTZ	Wideband alternating-phase low-power technique for zero residual splitting

Acronyms and symbols for isotopic composition

IRMS	Isotope ratio mass spectrometry
irm-NMR	Isotope ratio measured by Nuclear magnetic resonance
irm-MS	Isotope ratio measured by Mass spectrometry
LC-irm-MS	Liquid chromatrography coupled to isotope ratio measured by Mass spectrometry
GC-irm-MS	Gas chromatography coupled to isotope ratio measured by Mass spectrometry
CSIA	Compound-specific isotope analysis
PSIA	Position-specific isotope analysis
SNIF-NMR	Site-specific natural isotopic fractionation meausred by Nuclear magnetic resonance
f_i	Experimental isotopomer molar fraction as the ratio of the area of peak i to the total area of all peaks in the molecule determined by NMR
F_i	Statistical molecular fraction as the molar fraction for the carbon position i, in case of a homogeneous ^{13}C distribution within the molecule
δ	Isotopic composition (not to be confused with the chemical shift)
δ_g	Global isotopic composition as obtained by IRMS
δ_i	Isotopic composition at position i

^{h}E	Heavier isotopes of the element *E*
^{l}E	Lighter isotopes of the element *E*
R	Isotopic ratio
x	Isotopic abundance
E	Element
V-PDB	Vienna-Pee dee Belemnite
KIE	Kinetic isotope effect
EIE	Equilibrium isotope effect
α	Isotope effect
Δ	Isotopic fractionation
ε	Isotope enrichment
‰	Per mil, *e.g.* 1‰ = 0.1%

Other acronyms and symbols

API	Active pharmaceutical ingredient
C	Molar concentration
C_3	One of the three metabolic pathways for carbon fixation in photosynthesis
C_4	One of the three metabolic pathways for carbon fixation in photosynthesis
CAM	One of the three metabolic pathways for carbon fixation in photosynthesis (Crassulacean Acid Metabolism)
ETBE	Ethyl *tert*-butyl ether
E	Error due to partial saturation
IAEA	International Atomic Energy Agency
m	Weight, in NMR tube preparation
M	Molar mass
MDMA	3,4-methylenedioxy-N-methylamphetamine, commonly known as ecstasy

MTBE	Methyl *tert*-butyl ether
PCA	Principal component analysis
sn1	Substitution at position 1 of glycerol
sn2	Substitution at position 2 of glycerol
sn3	Substitution at position 3 of glycerol
TAME	*tert*-amyl methyl ether
TCE	Trichloroethene
TNT	Trinitrotoluene
VIM	International vocabulary of metrology
WHO	World Health Organization
ξ	Required accuracy
sinc	$\frac{\sin(a)}{a}$

1503

NMR based isotopomics